Oil-oil droplet deformation under DC electric field as a method to investigate clay electrorheology

Kjetil Hersvik

July 18, 2010

To Reidun

Abstract

Oblate deformation of silicone oil droplets when submerged in castor oil and subject to a DC electric field is measured and compared to predictions of the leaky dielectric model, with excellent agreement. Many uncertainties in the experiment remain, as well as uncertainty in determining parameters for the leaky dielectric model such as conductivity and interfacial tension. The main challenge encountered is movement of the droplet towards electrode at higher fields, which remains a paradox. The movement is studied carefully. Deformation when Laponite particles are added reveal processes with much longer time scales than the deformation of pure oil droplets.

Contents

Acknowledgements

I am very grateful for the opportunity to work in such a fine, international environment with friendly people and excellent lab equipment. My thanks go firstly to Professor Jon Otto Fossum, for his openness and generosity, as well as an encouraging and helping spirit. To Zbigniew (aka. Zbyscek) Rozynek, for his perseverance when helping me with any problem I may find myself stuck with, for team spirit, but sometimes also a much needed push to get things done instead of pondering problems all day long. My warmest thanks, also, to Paul Dommersnes who has visited from France twice, discussed on the phone on many occations, and written a hundred emails to me. He has had a vision for the project all along, and vested interest in all my findings, suggested many smart ideas, and helped me understand the physics on a deeper level.

Ole Tore Buset, our very own engineer, deserves to be saluted for his eagerness to assist in any way, technical or not. A special thank you also to Kristin Saeterboe who has taken drastic measures to find information and order supplies. For solving my long nightmares in measuring conductivity, I thank both Tore Loevaas and Arne Moholt with his electronic workshop crew.

And I would be embarrassed if not to extend my fullest gratitude to Andreas Lyng Nenningsland, Ph.D. candidate working in the Ugelstad Laboratory. He has joined me and helped me through all my experimenting needs with unfamiliar apparatus, be it measuring densities or interfacial tension. A complete stranger at first, he has always acted as a true friend.

1 Introduction

Deformation of droplets in electric fields is used in microfluidic applications, for example to induce droplet coalescence [2]. When it comes to the electrorheological (ER) droplets, research has suggested many uses for "smart" droplets that can be controlled, including soft displays, lab-on-a-chip for accurate chemical reactions or biological processes or even boolean logic for simple microfluidic computing [10]. Dielectric deformation of droplets can also be useful for understanding deformation of biological cells subject to electric field. Study of ER droplets can increase understanding of the ER effect which could be useful in dynamically controlled shock absorberes or electronic clutches, for instance. Study of clay physics is the common denominator in this research group, and the electrorheological properties of synthetic clay have been studied by group members, for instance with synchrotron X-ray scattering by Fossum et al. (2006) [9].

This study investigates oil droplet deformation when submerged in a second immiscible oil and subject to DC electric field, with emphasis on the oblate deformation arising when silicone oil is submerged in castor oil. Furthermore, Laponite clay is added to the silicone droplet, and the process of deformation is compared to pure oil droplets. A substantial effort is made to determine the conductivity of the fluids involved. Permittivity is measured, and different ways of measuring interfacial tension are also attempted.

2 Theory of Liquid Droplet Deformation in Electric field

In this section we will discuss pure liquid droplets subject to electric fields. The models discussed are natural starting points for the understanding of droplet deformation with the added electrorheological effect of clay particles. The notable pioneers in this field are O'Konski and Tacher who developed the perfect dielectric model (1954) [1], which predicts stretched (prolate) droplets. However, some experiments showed flattended (oblate) droplets. Theory for flattened droplets were developed by Taylor who introduced the useful leaky dielectric model (1966) [5]. Experimentalists as well as analytical and numerical physicists are still working to improve and verify the theory governing drop deformation in an electric field. Vizika and Saville [12] made strong experimental progress in 1992, and remain the most relevant study for comparison of theory and experiments. We start by calculating the electric field inside a dielectric sphere and the induced surface charge.

2.1 Dielectric sphere subject to electric field

In the following, we will calculate the resulting electric field for a rigid dielectric sphere embedded in a dielectric medium subject to a homogenous applied electric field. The derivation largely follows [3]. In a static case, the electric field E is related to the electric potential V as

$$\vec{E} = -\nabla V \tag{2.1}$$

Gauss' law from Maxwell equations reads

$$\nabla \cdot E = \frac{\rho}{\epsilon_0} \tag{2.2}$$

where ρ is the charge density and ϵ_0 is the vacuum permittivity. Since there are no free charges, operating with $\nabla \cdot$ and using equation (2.2) on equation (2.1) gives

$$\nabla^2 V = 0 \tag{2.3}$$

The electrostatic boundary conditions for a dielectric medium are

$$V_{in} = V_{out} \ , \qquad \text{at r = a} \tag{2.4}$$

$$\epsilon_{in}\frac{\partial V_{in}}{\partial r} = \epsilon_{out}\frac{\partial V_{out}}{\partial r} \ , \qquad \text{at r = a} \tag{2.5}$$

$$V_{out} \rightarrow -E_0 r\cos\theta \ , \qquad \text{for r} \gg \text{a} \tag{2.6}$$

where E_0 is the applied field far from the droplet and θ is the angle from the direction of the electric field through the center of the sphere.

The solution of Laplace equation, Eq. (2.3), with the above boundary conditions on a homegenous dielectric sphere of permittivity ϵ_{in} surrounded by homogenous dielectric material of permittivity ϵ_{out} is derived in Appendix A.1. It follows that the potential inside the sphere is

$$V_{in}(r,\theta) = -\frac{3\epsilon_{out}E_0}{\epsilon_{in}+2\epsilon_{out}} r\cos\theta = -\frac{3\epsilon_{out}E_0}{\epsilon_{in}+2\epsilon_{out}} z, \tag{2.7}$$

giving a uniform electric field inside the sphere:

$$\vec{E} = \frac{3\epsilon_{out}}{\epsilon_{in}+2\epsilon_{out}}\vec{E}_0 \tag{2.8}$$

or with $G \equiv \epsilon_{in}/\epsilon_{out}$:

$$\vec{E} = \frac{3}{G+2}\vec{E}_0 \tag{2.9}$$

The field is illustrated in Fig. 1.

The potential outside the sphere is (refer to Appendix A.1)

$$V = \frac{B_1\cos\theta}{r^2}. \tag{2.10}$$

The potential of a dipole field is

$$V = \frac{p\cos\theta}{4\pi\epsilon_0 r^2}. \tag{2.11}$$

Therefore the total dipole moment of the sphere is

$$\vec{p} = 4\pi\epsilon_0\frac{\epsilon_{in}-\epsilon_{out}}{\epsilon_{in}+2\epsilon_{out}}a^3\vec{E}_0 \tag{2.12}$$

where we have used Eq. (A.17).

The polarization $\vec{P}$ inside the sphere is constant (like the electric field). The total dipole is the volume integral of the polarization, therefore

$$\vec{P} = \frac{p}{\frac{4}{3}\pi a^3} = 3\epsilon_0\frac{\epsilon_{in}-\epsilon_{out}}{\epsilon_{in}+2\epsilon_{out}}\vec{E}_0. \tag{2.13}$$

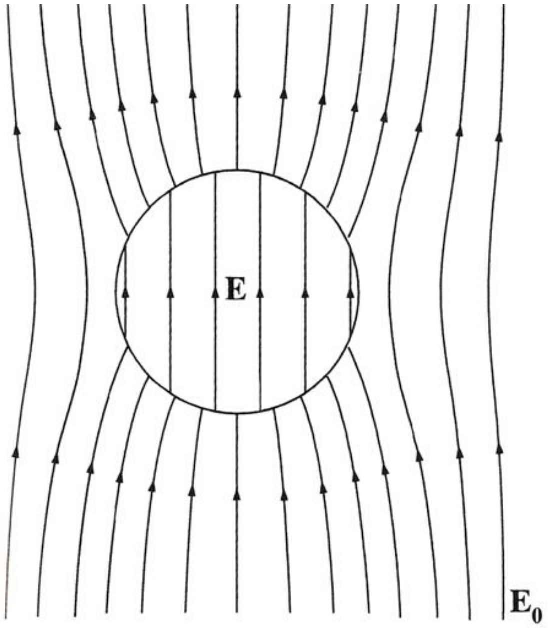

Figure 1: Electric field inside and outside of a dielectric sphere when a homogenous electric field E_0 is applied. Illustration from [3]

The polarization vector is $\vec{P} = P\hat{z}$, where $\hat{z}$ is the unit vector parallel to the $\vec{E}_0$. The polarization charge on the surface of the sphere is

$$q_\sigma = \vec{P} \cdot \hat{n} = P \cos\theta \tag{2.14}$$

where $\vec{P}$ is given by Eq. 2.13. This gives positive surface charges on one pole and negative surface charge on the other pole.

2.2 The perfect dielectric model

In a study of aerosol droplet distortion by O'Konski and Thacher in 1954 [1], the authors successfully approximated the deformation of insulated droplets in a constant electric field E by minimizing the sum of surface energy and electric potential energy of the ellipsoid. Allan and Mason achieved the same in 1962 by balancing surface and electric stress. The electric field acts on the polarization charges given in Eq. (2.14), causing the droplet to stretch along the field direction.

Deformation of a droplet has been defined by

$$D = \frac{d_{\|} - d_{\perp}}{d_{\|} + d_{\perp}} \tag{2.15}$$

where $d_{\|}$ is the length or diameter of the drop in the direction parallel to the electric field and $d_{\perp}$ is the diameter in the direction perpendicular to the electric field.

The result for small deformations D of a *dielectric drop* with a dielectric medium outside the drop is [4]:

$$D = \frac{9}{16}\frac{a\epsilon_{out}\epsilon_0 E^2}{\gamma}\frac{(\epsilon_{in}-\epsilon_{out})^2}{(\epsilon_{in}+2\epsilon_{out})^2} \tag{2.16}$$

where ϵ_{in} and ϵ_{out} is the relative permittivity inside and outside the drop, respectively, ϵ_0 is the vacuum permittivity, γ is interfacial tension and a is the drop radius. The degree of deformation D is essentially given by a competition between surface tension γ, which favors a spherical droplet, and electrostatic forces that stretch the droplet. For a *conductive drop* in a dielectric medium, the expression reduces to:

$$D = \frac{9}{16}\frac{a\epsilon_{out}E^2}{\gamma}. \tag{2.17}$$

Note that since the deformation is dependent on E^2, the deformation is the same when the electric field E is reversed, owing to symmetry in the droplet shape. Furthermore, both expressions are strictly positive, describing an elongation of the drop in the electric field resulting in a prolate shape. However, experiments by Allan and Mason (1962) found cases where the drop deformation was negative, i.e. an oblate deformation shape resulting from shortening in the field direction [4]. A new model was needed to incorporate this behavior.

2.3 The leaky dielectric model

In 1966 Taylor adressed the issue of oblate deformation with what has been called the *leaky dielectric* model. He realized that no matter how small the conductivity of the surrounding liquid is, charge will be able to reach the drop interface. The free charge build up at the drop interface makes the tangential component of the electric stress nonzero, and viscous flow is induced to balance this tangential force.

The electrostatic approximation can safely be utilized in this model since the characteristic time for electric processes, $\tau_C \equiv \epsilon/\sigma$, is much greater than the characteristic time for magnetic processes, $\tau_M \equiv \mu\sigma l^2$ [4]. A more delicate assumption, however, assumes that the electric potential of the drop is the same as in the case of static charge [5]. Fluid currents challange this assumption by causing charge convection, but in most cases the transport time scale is sufficiently long compared to the time scale for electric processes which counteracts the charge migration [4].

The electric potential V_{in} inside and V_{out} outside of a *conducting sphere* in the static case is known and behaves strikingly similar to that of a insulated dielectric sphere calculated in Section 2.1, and is given by [5]

$$V_{out} = E_0\cos\theta\left(r + \frac{1-R}{2+R}\frac{a^3}{r^2}\right) \tag{2.18}$$

$$V_{in} = E_0 r\cos\theta\frac{3}{2+R} \tag{2.19}$$

where $R \equiv \sigma_{in}/\sigma_{out}$ is the ratio of conductivity inside over that outside the drop. The fluids are assumed to exhibit ohmic resistance. The resulting electrical field therefore has the same shape as for the dielectric sphere shown in Fig. 1.

Accumulation of free surface charge can be appreciated by balancing the current in the two phases with different conductivities σ_i [4]. Assume the system has no net charge, so before the electric field is applied, everything is neutrally charged. If the conductivity inside the drop is highest, applying the electric field will allow charge carriers inside the drop to travel faster than outside the drop. At the interface, charge builds up causing a reduced field inside the drop. When the current on both sides of an interface are equal, the system is stationary. If the conductivity inside the drop is lower than that of the surrounding phase, charge will build up to enhance the field inside the drop, and the current in the two phases become equal when the system is stationary, just the same.

The component of the electric field tangential to the drop interface must be continuous across the boundary. At the interface, the field in any tangential direction is thus the projection of the homogenous field inside the drop onto a chosen vector tangential to the interface. It is then clear that the tangential field is zero at the two ends ($\theta = 0, \pi$) where the surface is orthogonal to the electric field, however as the interface curves back, the tangential component becomes non-zero. With free charge carriers accumulated on the interface, these will cause a tangential electric stress along the surface. In the equatorial plane, at $\theta = \pi/2$, there is naturally no charge buildup and therefore no tangential electric stress even though the tangential component of the electric field is strongest here.

Viscous flow is necessary to balance tangential electric stress, since surface tension is only acting normal to the interface. The tangential electric stress on the charge carrying species couples into fluid flow in the same direction as the electric stress. Viscosity in the fluid flow produces a drag in the opposite direction which becomes the balancing force along the surface. The direction of fluid flow is determined by the sign of β [5]

$$\begin{aligned} \beta &= R - G \qquad \text{or equivalently} \\ \beta &= \frac{\sigma_{in}}{\sigma_{out}} - \frac{\epsilon_{in}}{\epsilon_{out}} \end{aligned} \tag{2.20}$$

when $G \equiv \epsilon_{in}/\epsilon_{out}$. $R \equiv \sigma_{in}/\sigma_{out}$ as before. Consider $\sigma_{in} < \sigma_{out}$. In this case the free surface charge accumulated in the polar ends ($\theta = 0, \pi$) has a polarity such that it is drawn toward the equatorial region ($\theta = \pi/2$). The stream lines thus head in the same direction, from the poles towards the equator as shown in Fig. 2, where the ratio of permittivities G is chosen so that the competing effect of permittivity difference in ϵ_{in} and ϵ_{out} is assumed to keep the spherical droplet shape intact. This flow direction, when $\sigma_{in} < \sigma_{out}$, causes a stress contribution towards an *oblate* shape, meaning expansion in the equatorial region. In the opposite case, when $\sigma_{in} > \sigma_{out}$, the flow direction causes stress that will contribute towards a *prolate* shape, meaning elongation of the drop in the field directon.

Understanding that both a difference in relative permittivity ϵ_i and conductivity σ_i over the drop boundary contributes to shape deformation, the combined effect on drop deformation D is summarized by the following equations[12, 13]

$$\begin{aligned} D &= \frac{9}{16} \frac{a \epsilon_{out} \epsilon_0 E^2}{\gamma} \frac{\Phi}{(2+R)^2} \\ \Phi &= R^2 + 1 - 2G + \frac{3}{5}(R - G)\frac{2 + 3\lambda}{1 + \lambda} \end{aligned} \tag{2.21}$$

where $\lambda \equiv \mu_{in}/\mu_{out}$ is the ratio of viscosity inside and outside the drop respectively, ($G = \epsilon_{in}/\epsilon_{out}$ and $R = \sigma_{in}/\sigma_{out}$ as before). From this, one realizes that

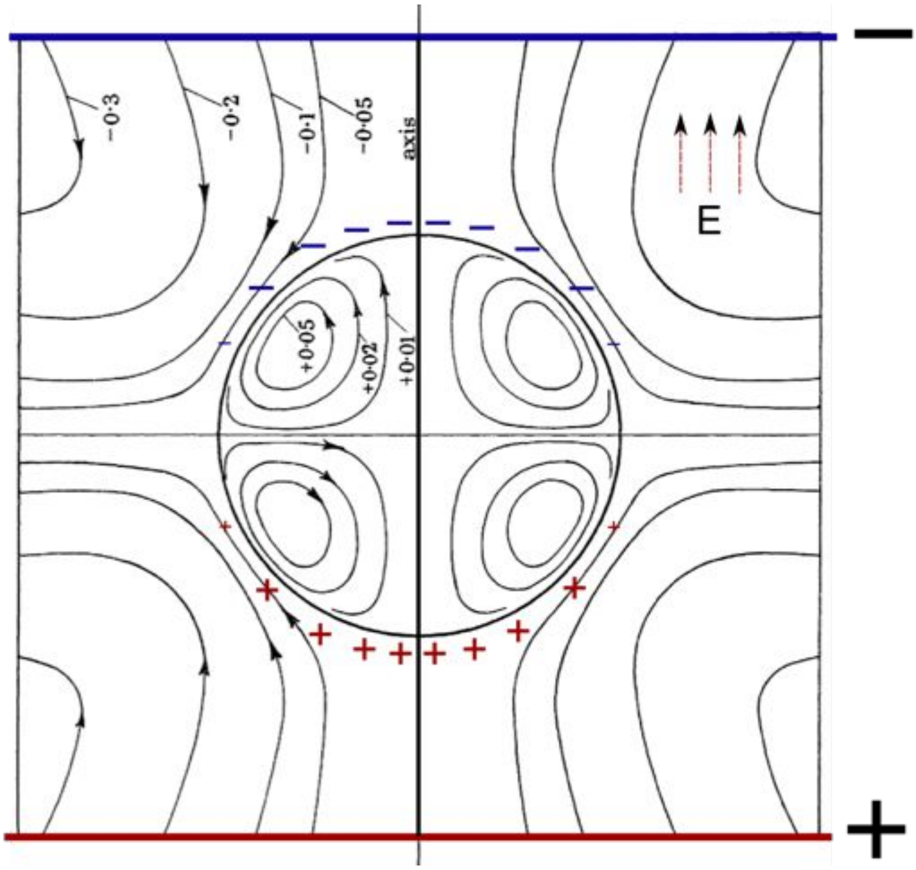

Figure 2: Streamlines of vicous flow when $\beta < 0$. Parallel electrodes run at the top and bottom of the figure creating a uniform electric field indicated by E. Free surface charge accumulation that causes fluid flow is indicated with + and - sign around the surface. Illustration adapted by author from [5].

the existance of even a small conductivity in the surrounding oil enables charge accumulation, and a lower conductivity inside the drop compared to outside is a necessary condition to produce an oblate drop shape in an electric field. A difference in relative permittivity, on the other hand, will always contribute to prolate deformation, and can possibly dominate such that even when the conductivity is higher outside the droplet, the resulting deformation is prolate.

2.4 Validity of the Leaky Dielectric Model

The relation of droplet deformation to the various parameters (a, ϵ, E, γ, σ) in the leaky dielectric model is qualitatively accurate. However the quantitative accuracy has a tendency of systematic error, suggesting that the coefficient in the deformation expressions is flawed[4]. Improvements have been made with extended analytical and numerical models.

Also, one should expect that the limit $\sigma_{in,out} \rightarrow 0$ yields the perfect dielectric model. Clearly, this is not the case as only the ratio of conductivities R enters the equation of the leaky dielectric Model. The ratio R could for instance be equal to unity in both the limit of high conductivities and and the limit of vanishing conductivites. The physical cause of the inconsistency in the limit of vanishing conductiviy is due to finite thermal charge spreading at the interface [6]. The assumption by Taylor that electric charge is sharply confined to the interface breaks down at small conductivities. Zholkovskij et al. (2002) [6] derived a more general analytic model to bridge the perfekt and the leaky dielectric models by solving the Poisson equation $\nabla^2 V = -\rho/\epsilon$ instead of Laplace equation.

Baygents & Saville (1989) also proposed an electrokinetic model for larger deformations by taking into account charge diffusion on the micro-level, however the prediction for drop deformation ended up equal to the that for the leaky dielectric model [4, 7].

A promising correction to the leaky dielectric model is the correction due to charge convection investigated computationally by Feng (1999) [7]. It predicts enhanced prolate deformation and reduced oblate deformation in better agreement with the experimental reports. The cause of this is that electrical charges are convected by fluid flow and viscous flow diminishes. The electric Reynolds number Re_E, defined as the ratio of the time-scales of charge convection and charge conduction, indicates the importance of charge convection effects. Re_E has been assumed sufficiently small, however charge convection effects which reduce flow effects, are prominent even at charge relaxation time-scale of $\sim 10^{-3}$s [7].

3 Clay and electrorheology

In recent years, clay has been an active research field within experimental and theoretical physics. Accessibility and interest has grown as a result of abundance in clean chemistry customized synthetic clays, and research activity includes incorporating clay into modern material science in combination with other synthetic and complex adaptive materials such as colloids, polymers, liquid crystals and bio materials [8].

Laponite is one of the most widely studied synthetic clay. It is called a smectite clay, meaning that it has a $2:1$ structure; a 1 nm thick platelet consisting

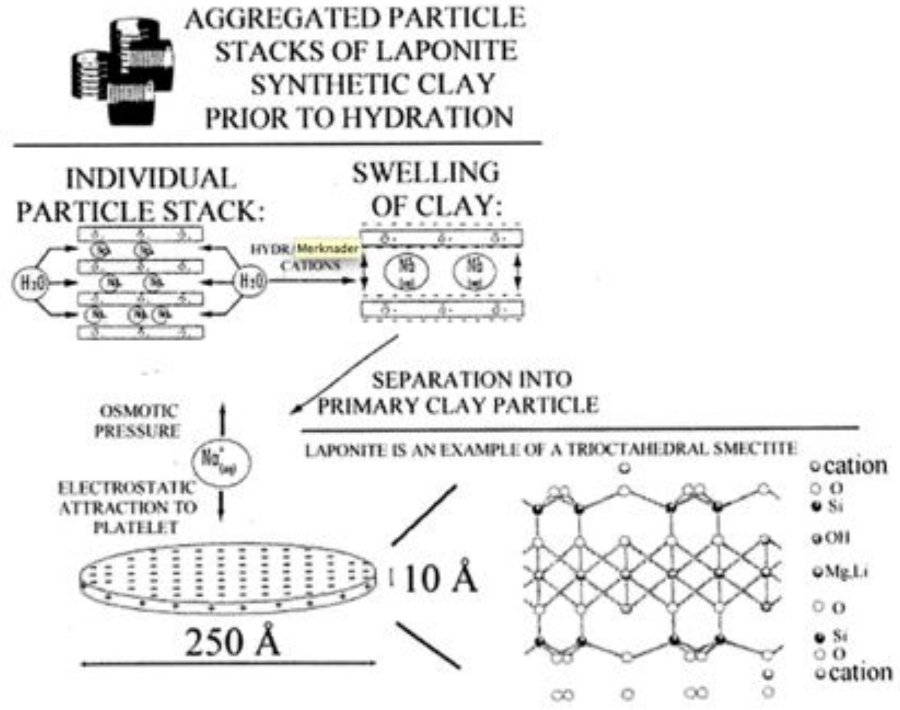

Figure 3: Illustration of Laponite at various scales; first, aggregated laponite stacks; second, individual stacks consisting of platelets with intercalation ions; third, swelling of stack as a result of hydration - water intercalates between platelets; fourth, individual platelets after gelation; finally, the crystal structure of each plateletel consisting of three silica sheets. Via [8].

of two tetrahedral silica sheets sandwiching one octahedral silica sheet. The 1 nanometer thick platelets may individually be considered as single crystals. In the dry state, the platelets stack like a deck of cards by sharing charge-compensating cations. Laponite is a swelling clay, meaning that water can intercalate between platelets in the stack as seen in Fig. 3. This is useful in industrial applications, etc., and is contrasted by natural clay in the ground which is non-swelling. A simplifying advantage of Laponite is the mono dispersity of colloidal platelets; the plate particles that separate when dissolved are of equal, 25 nm diameter. Other synthetic clays such as Fluorohectorite as well as natural clays are polydisperse and micrometer sized. In the dry state the stacks made up of platelets tend to aggregate into larger grains [8].

3.1 Chain formation

The study of nanolayered smectite clay particles subject to a strong external electric field have shown fast and extended structuring. The orientation is understood by interaction of induced electric dipoles, since only particles with suitable polarization properties align into chain formations. X-ray scattering studies[9] have shown that the particles polarize and align along the silica sheets. The mechanism of polarization is not fully understood, but two important factors include the so-called interfacial polarization as well as electric anisotropy of the particle. The particle rotation and orientation in the electric field dictates a structural attachment of the induced dipole to the particle shape. A slight reduction of plate separation in electric field suggests that intercallated ions and perhaps water dominate the interfacial polarization process for smectite particles. This would be consistent with the fast response to electric field [9].

4 Experiments

4.1 Deformation measurement

4.1.1 Oil samples and density

Two silicone oils and two plant oils are used in this study. The silicone oils are 10 and 100 cSt viscosity respectively, both "Dow Corning 200" products. The plant oils are delivered by Sigma-Aldrich Norway AS, and consist of castor oil (Fluka 83912) and corn oil (Sigma C8267).

The choice of oil samples is inspired by the experimental investigation included in the original paper by Taylor[5]. In the paper, a silicone oil is reported for the drop phase while a weak concentration gradient of castor oil and corn oil is reported as the outer phase, in order to neutralize buoyancy. This technique is replicated here with a 10 cSt silicone oil drop, while two slightly different mixtures of castor and corn oil are used as starting point for the concentration gradient. The oil samples are listed in the table below with measured densities performed at the Ugelstad laboratory on campus.

Sample	Manufacturer density (kg/L)	Measured* density (kg/L)
50% Castor-, 50% Corn oil	(0.900 + 0.961)/2	0.9351
10cSt Silicone oil	-	0.9328
Castor oil	0.961	0.9600
100cSt Silicone oil	0.964**	0.9670

*) Densities are measured on an Anton Paar DMA 5000 density meter, with originally 6 significant digits. Castor oil and 100cSt silicone oil were measured on an an older repair replacement model with only the 4 significant digits reported here.

More commonly, a slightly denser and more viscous 100 cSt silicone oil is used for drop phase with pure castor oil as outer phase, without density gradient. The oils are listed in the table above. This choice simplifies the uncertainty of the distribution when mixing two similar concentrations of castor and corn oil together. The disadvantage is that the drop sinks gradually, however the rate is very slow thanks in part to the high viscosity of the castor oil.

4.1.2 Drop-host sample cell

Three sample cells are used. Firstly, a set of copper electrodes are designed to fit inside plastic cuvettes of cross section 10x10mm. Electrode separation is 8.2mm. The cell is used for the 100 cSt silicone drop in pure castor oil. The advantages are long falling heights for the droplet (a few centimeters depending on the oil level, etc), as well as easy electrode cleaning and abundant replacement plastic cuvettes. A variation of this cell has electrodes placed on the outside of the plastic cuvettes with a 1mm air gap, resulting in electrode separation of 13.5mm. The outside electrodes are only used for comparison, while standard procedure is to use electrodes on the inside of the fluid container. Thirdly, a cubic sealed plexiglass sample cell is designed with copper electrodes incorporated. The inside lengths are 10mm, and the electrode separation is more specifically 9.9mm. This sample cell is filled with castor oil and corn oil gradient, and has the possibility to view the deformation from above through the transparent lid.

4.1.3 Setup

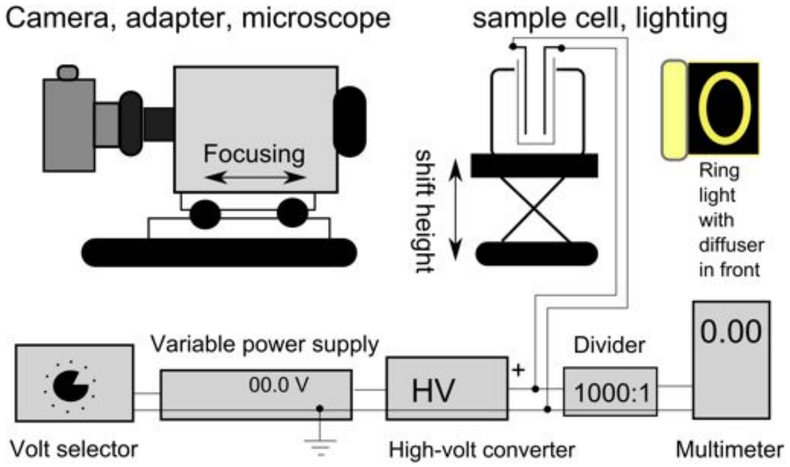

Figure 4: Deformation measurement setup:

A Canon 550D digital SLR camera, mostly used in full HD video mode rather than taking photos, is connected to the Zeiss Stemi 2000-C microscope with an adapter set delivered from Zeiss. The camera is aligned with reference to a hanging stick. The microscope can shift horizontally in order to focus. The sample cell is mounted on a vertically shifting base to adjust height if the droplet falls out of the frame between measurements. The sample cell is lighted from behind by a ring light with a translucent plastic dish in front as diffuser.

A self made voltage selector is used for analog programming of the Delta Elektronika ES 030-5 (0 - 30 V) power supply. A fixed discrete range of electric field values saves a lot of work when repeating measurements and makes quickly switching between applied potential differences possible without the need to write down every potential difference value. The selector is essentially a potential divider consisting of a series of 10 similar 500 Ω resistors, with a 20 kΩ variable resistor on the end connected to ground, and a 200 kΩ variable resistor connected to the 5 V reference pin of the power supply. An 11 step switch connects the analog programming pin of the power supply to each of the evenly spaced, non-zero potentials available in the chain. Thus, the highest and lowest potential difference can be set by iteratively adjusting the variable resistors. The intermediate steps are evenly distributed to the extent that the metallic film resistors of 500 Ω are homogenous from production.

The high-volt converter converts a range of 0 -15 V into 0 - 5 kV (DC). It is assembled by the electronic workshop of the institute. The output is checked, and it is a linear function of the input signal, with a bend towards zero below 300 V output. Nevertheless, the final output of each of the 11 selectable potential differences is recorded with a multimeter connected via a 1000:1 potential divider, and these values are used in the analysis. The potential divider is designed for impedance match with the high-volt converter.

Not included in the setup overview, Figure 4, is an on-off switch for the applied potential difference, which is connected to a light emitting diode next to the sample cell. When the potential difference is off, the LED turns on, and a reflection from the red diode is seen in the droplet. To know the exact video frame in which the field is turned on is a great aid for data processing and is vital for determining starting point when studying dynamics.

4.1.4 Electric noise

The high-volt signal is found to be quite noisy. The noise can be seen in Figure 5 and Figure 6, which shows the response time for turning the potential difference on and off, respectively. The amount of noise is striking, however the droplet system never shows any effect of the noise. The potential difference is not determined from the oscilloscope, but a multimeter which takes the DC average without showing any instability.

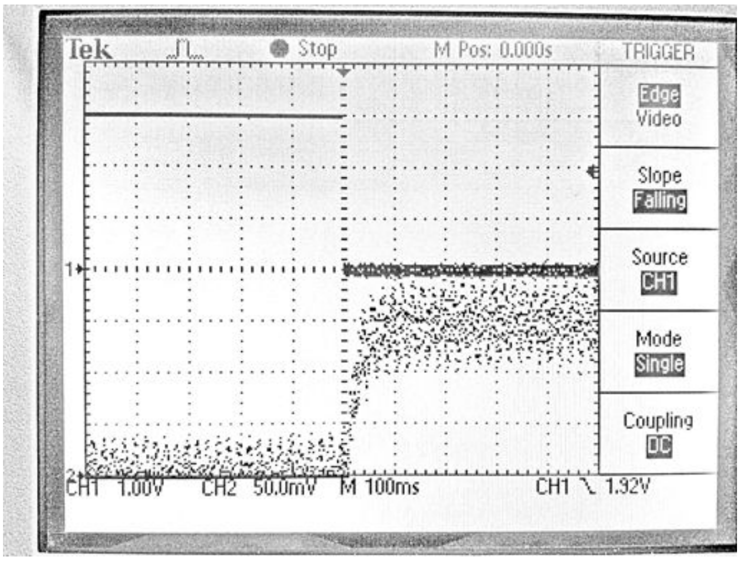

Figure 5: Potential difference response when signal is switched on. The LED lamp is turned off as indicated by the step in the dark horizontal line. Response time is around 100 ms.

4.1.5 Data acquisition and processing

Images are normally obtained from a video sequence captured by the SLR camera. Thus, the first step is to select the relevant frames for measuring droplet deformation. The level of applied potential difference is announced in the audio track. The uses of switches to control the potential difference can be heard in the recording and aids timing of the measurements. The most recent measurements are also aided by the red light emitting diode which identifies the exact frame when the field is applied.

Once the frames are selected, measurement of the deformation D defined in Eq. (2.15) is performed by a MATLAB script developed for the project by Rene Castberg, Physics Ph.D. candidate at University of Oslo. The border of the droplet is detected as shown in Figure 7. The position, width, height and area of the droplet is output to a text file, in addition to a few other parameters.

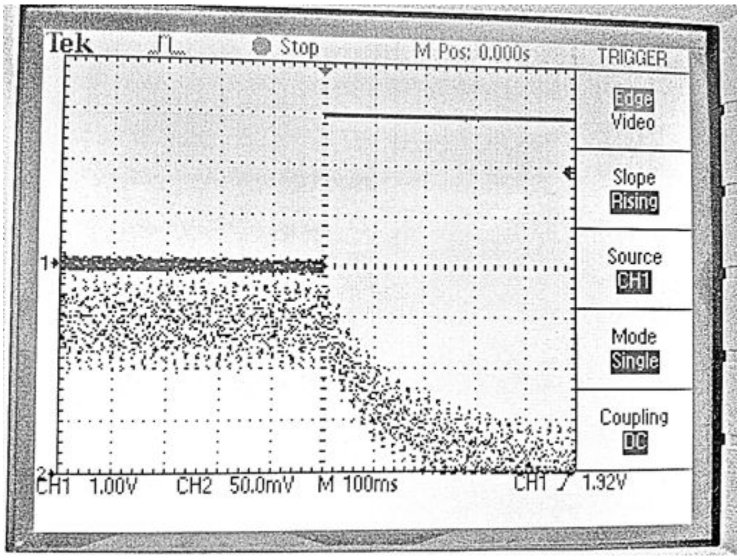

Figure 6: Potential difference response when signal is switched off. The LED lamp is turned on as indicated by the step in the dark horizontal line. Response time is around 400 ms.

4.2 Conductivity measurements

Conductivities of the oil drop and the surrounding oil are perhaps the two most vital parameters in order to predict the deformation behavior of the drop. As pointed out in the review by Saville[4], only a limited number of fluids have previously been studied for drop deformation, and even in these cases, "conductivities have not been controlled". The leaky dielectric model takes into account the fact that the fluids are not quite electrically isolated. The electric conductivity is nevertheless very weak, and thus challenging to measure.

4.2.1 Conductivity sample cell

A custom made sample cell is used to contain the fluid while measuring its electric conductivity. The sample cell is made from two plates of plexiglass, each carved so that when attached along the flat side give an open container with a height $h = 27.4$ mm and width $w = 11.4$ mm. Two electrodes with the same height and width measurement are glued to the walls, and the resulting electrodes separation is $d = 2.10$ mm (± 0.05). By measuring the resistance R across the sample cell, the conductivity of the fluid is given by

$$\sigma = \frac{1}{R}\frac{d}{w \cdot h}. \tag{4.1}$$

4.2.2 Measuring high resistance

Since the fluid is nearly electrically isolating, the resistance across the cell is very high and in the order of 100 GΩ, despite the small electrode separation. The best achieved method for determining the resistance across the cell is to

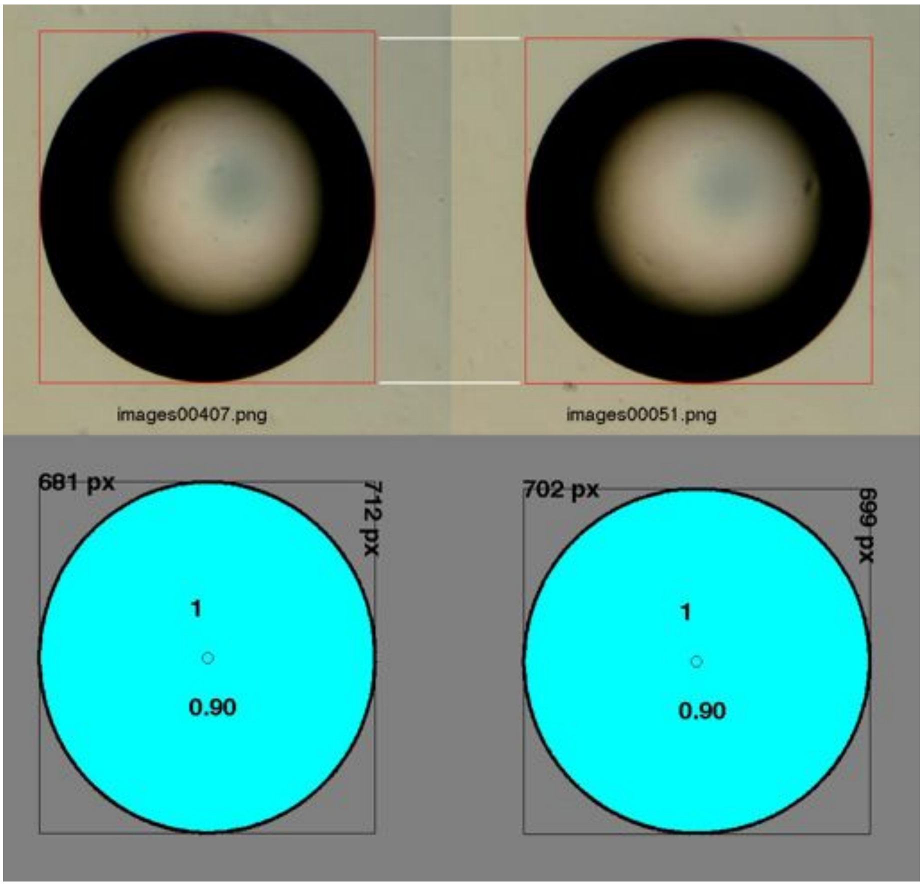

Figure 7: Images included in the output of the Matlab script which automatically measures deformation for a batch of images. The first droplet has a relatively weak oblate deformation of $D = -0.022$, while the second is a typical non-deformed droplet (slightly prolate).

apply a substantial potential difference across the electrodes while measuring the current going through it with a sensitive picoammeter. A preceding electric design involved a Wheatstone bridge with high resistance ratios across each bridge, and equally high ratio of resistance between the two parallel bridges. The highest resistance would be the sample cell, and by adjusting the other resistors until the potential difference across each bridge midpoint was zero, the sample cell resistance could be determined from the value of the other resistors. The idea was a triumph, however noise control is easier with the simplest possible circuit, namely the current measurement through the cell when a high potential difference is applied.

4.2.3 Choice of voltage

The applied voltage levels in conductivity measurements are chosen so that the resulting electric field levels in the cell are in the same range as those for deformation experiements in larger cells. The drop deformation is typically studied systematically in the electric field range of 300-2000V across 8.2mm or 10mm. In other words, up to 250 V/mm. The picoammeter can only handle 220 V, corresponding to 105 V/mm in the cell. In order to check the conductivity as a function of electric field intensity in sufficiently high electric field range, a protective resistor is demanded so that in case of an electric break down, i.e. spark, through the measurement cell, the expensive picoammeter is not destroyed. After protective measures have been taken, the highest voltage applied in conductivity measurements is set at 600 V, corresponding to 286 V/mm.

4.2.4 Setup and circuit

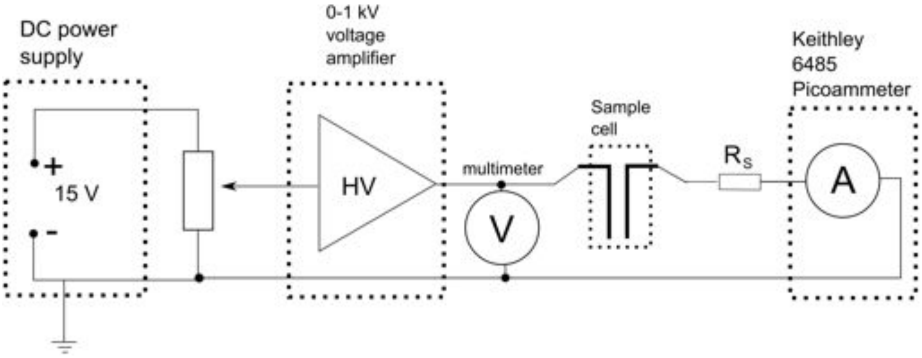

Figure 8: Conductivity measurement setup

An overview of the setup is shown with circuit symbols in Figure 8. An old power supply generates the initial 15 V DC signal which is adjusted with a standard 20 turn variable resistor of 1 kΩ. The high-volt converter is assembled by the electronics workshop at the institute and converts 0-12 V into 0-1 kV (DC). The output from the high-volt converter is monitored by a multimeter which can cope with 1 kV potential difference. The high-volt signal is then connected to one of the electrodes of the sample cell. In case of electric breakdown in the cell, a 6.8 MΩ protective resistor R_S is inserted between the low potential electrode and the Keithley 6485 picoammeter. The protective resistor is sufficiently power and voltage rated according to the operations manual of the picoammeter.

4.2.5 Noise

The noise in the picoammeter measurement is reduced from aproximately 20 pA to 2 pA by exchanging the BNC coaxial cable provided by the manufacturer with very short regular banana cables from the lab. The noise signal is measured even though the power supply for the applied potential difference is off, and even if the banana cables are removed. However, when removing the BNC-to-banana adapter from the connector on the picoammeter, the noise signal is small enough to be completely filtered by the digital median filter.

A digital median filter setting of rank 5, corresponding to displaying the median of the 11 most recent readings is used. (Measurement rate is observed to be ∼300ms per measurement). The noise of the picoammeter has not been the most limiting factor in any of the measurements in this study, however. Uncertainties are further disussed in the Analysis, Section 5.2

4.2.6 Cleaning the sample cell

Before cleaning, the sample cell is dismounted into the two flat pieces. Each part is brushed with detergent and rinsed of repeatedly in tap water. Afterwards, they are put in a strong ultrasonic bath until a tiny cloud-like substance no longer comes off. The parts are rinsed again in tap water, and dried off with pressurized air from a hose.

4.3 Permittivity measurement

Permittivity measurements are performed in the same sample cell as in conductivity measurements. The capacitance of the cell with and without fluid is measured directly using the Agilent 4263B LCR meter. The cables are 1m long kelvin clip cables manufactured for the apparatus. Other than the necessary 1m cable length setting, default settings are used, and both open circuit and short circuit correction procedure is performed prior to measurement.

The probe frequencies are 100 Hz and 1 kHz, and the probe level was 1000 mV. The capacitance measurement at 1 kHz probe frequency has three significant figures and was preferred over the 100 Hz probe frequency measurement which has 2 significant figures. The 100 Hz probe frequency is paid attention to, since the frequency is closer to the desired zero-frequency limit which should be used to calculate static relative permittivity. The relative permittivity is easily calculated from

$$\epsilon_r = \frac{C_{sample}}{C_{empty}} \tag{4.2}$$

where ϵ_r is the relative permittivity of the sample, C_{sample} and C_{empty} are capacitance measurements for sample cell with and without sample, respectively.

4.4 Interfacial tension measurement

Interfacial tension is a force per unit length tangential to an interface, similarly to surface tension for a surface. It is the force that returns the droplet to a spherical shape after it has been deformed.

Figure 9: Pendant drop hanging from a burette with tip diameter of 4mm. 100 cSt silicone oil drop in sunflower oil (!).

The first attempt to measure the interfacial tension was to create a pendant drop setup. The hope was that the small difference in densities of the two oils would allow a substantial sized oil droplet of the heavy phase to hang from a burette submerged in the light phase. However, the drop was very small, as can be seen in the photo of Figure 9, and determining the volume was highly uncertain. The relatively high viscosity of the oil also required a long relaxation time to reach static equilibrium after expanding the drop. In sum, the droplet detached from the burette when it was less than pea-sized, and the bridge attaching to the burette was highly unstable in diameter.

The second attempt to determine the interfacial tension was performed on the Tensiometer at the Ugelstad laboratory on campus. The apparatus utilizes the ring method introduced by Lecomte and du Noüy in 1919 [14]. In the ring method, the light phase is floated on top of the heavy phase. Illustrative photos are in Figure 10. A horizontal ring is submerged in the heavy phase and pulled very gradually through the interface of the two phases. The force on the ring is graphed, and the peak value is recorded relative to the initial weight pulling on the ring. The surface tension is ideally the force of the meniscus divided by the inner and outer circumference of the ring, however since the geometry of the meniscus is non-vertical, corrections need to be made. Both Zuidema and Waters [15], and Huh and Mason [16] have provided correction methods, where the latter has proven to be most successful. The corrections are based on parameters such as densities and viscosities of the phases. Unfortunately, the interfacial tension was too small for the threshold of the Tensiometer to interpret the result, however a screenshot of the graph was obtained for the 10 cSt silicone oil interface with the even mix of corn and castor oil. In the case of the 100 cSt silicone oil interface with pure castor oil, the arrangement of light phase on top of the submerged ring was unsuccessful altogether.

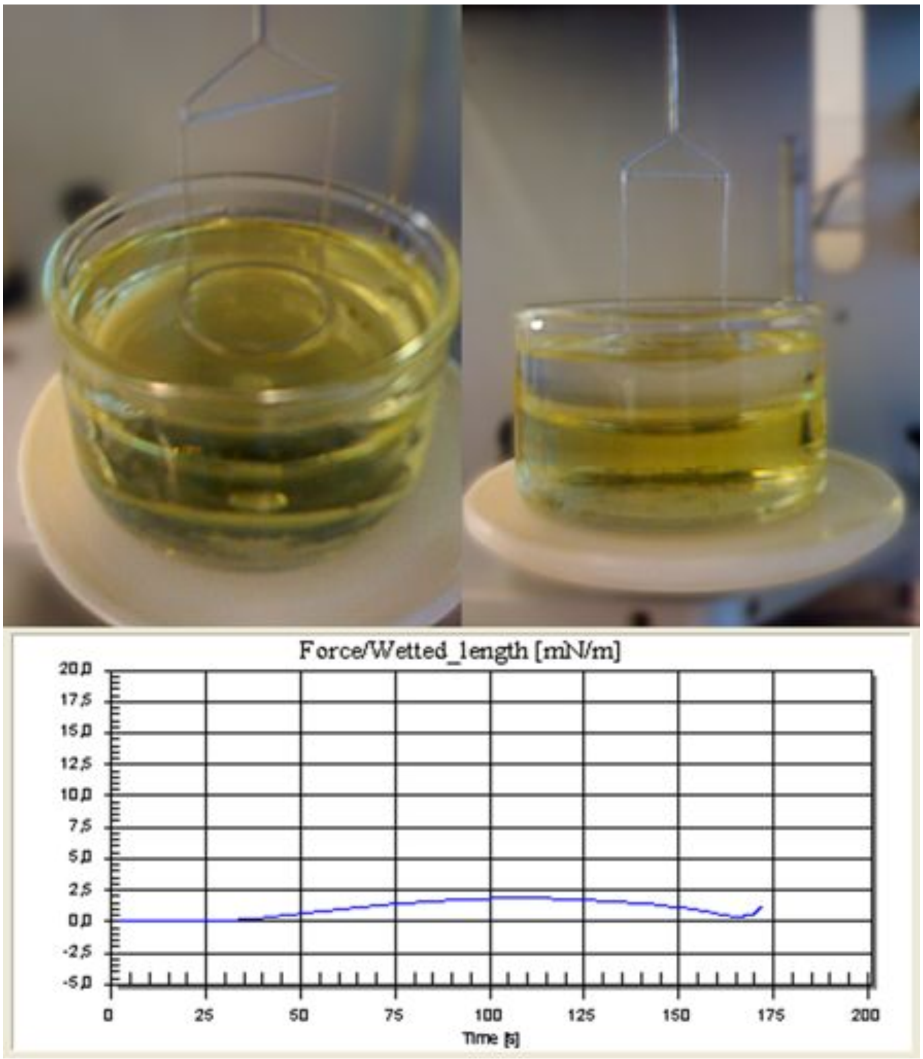

Figure 10: Teniometer sample photos and graph of interfacial tension from 10 cSt silicone oil interfacing with an even mix of corn and castor oil. The graph shows the uncorrected force on the ring per ring circumference. The peak is seen at $\sim 2 \cdot 10^{-3}$ N/m, however correction for non-vertial meniscus have not been applied and can alter the measurements up to a few tens of percent.

5 Analysis and Results

5.1 Deformation

5.1.1 Pure silicone oil droplet in Castor oil

Thorough investigation of the deformation of pure oil droplets is important for understanding the basic mechanisms of deformations, as well as verifying the experimental setup against other studies. A plot from the attempt of using a gradient of castor and corn oil is included in Appendix A.4, Figure 30, however the simplicity of using pure castor oil with 100 cSt silicone droplet prevailed. In the experiment performed with surrounding oil gradient, nonetheless, observations were made of the effect of droplet motion on droplet deformation for both horizontal and vertical movement. The horizontal movement is widely expected to be due to small net charges, while circulation patterns when close to electrode are likely candidates for cause of vertical movement. Anyhow, horizontal movement reduced the oblate deformation while vertical movement enhanced the oblate deformation.

Deformation D as a function of the squared electric field multiplied by drop radius aE^2 is plotted in Figure 11 for the collection of 100 cSt silicone droplets in pure castor oil. The lower range behaves as predicted by linear electrohydrodynamics, and a linear regression is performed for the readings where the electric field is less than 130 V/mm. Figure 12 shows all of the subplots of Figure 11 in one window, and with the axis used, the points should ideally collapse along the same straight line. The consistency between each of the five droplets is quite reasonable, indicating fairly good repeatability.

Horizontal movement is believed to be responsible for a lot of the discrepancy observed when more than 130 V/mm electric field is applied. 130 V/mm is the field value for which movement towards either electrode becomes obvious. The deformation is reduced at higher field strengths, in agreement with the observed effect of horizontal movement compared to vertical movement. For the last droplet, P008, the velocity was carefully measured at each applied electric field, and the result is shown in Figure 13. The velocity as a function of E^2 increases quite steadily, however in Figure 14 one can se how the velocity is non-linear, almost non-existing up until 130 V/mm (1000 V/8mm). This figure also includes the falling velocity of the droplet, which is perceived to be quite small.

The movement of the droplet towards electrodes at higher field values is a bit of a paradox. Any net charge on the drop should be neutralized due to conductivity of the fluids. No considered processes, such as fluid flow or conductivity changes, exhibit any effect resembling spontaneous symmetry breaking, but rather a charge balancing effect. Startled by the nonlinearity of the velocity as a function of applied field, a series of experiments was performed to measure the relation, and plots are included in Appendix A.2.

Deformation as a function drop size is evaluated for the same set of five droplets by plotting the slope of each linear regression against raidus a of the drop. The result is seen in Figure 15 and is supportive of the expected linear relation of deformation to drop radius. The plot gives an in indication of amount of inter-sample random error.

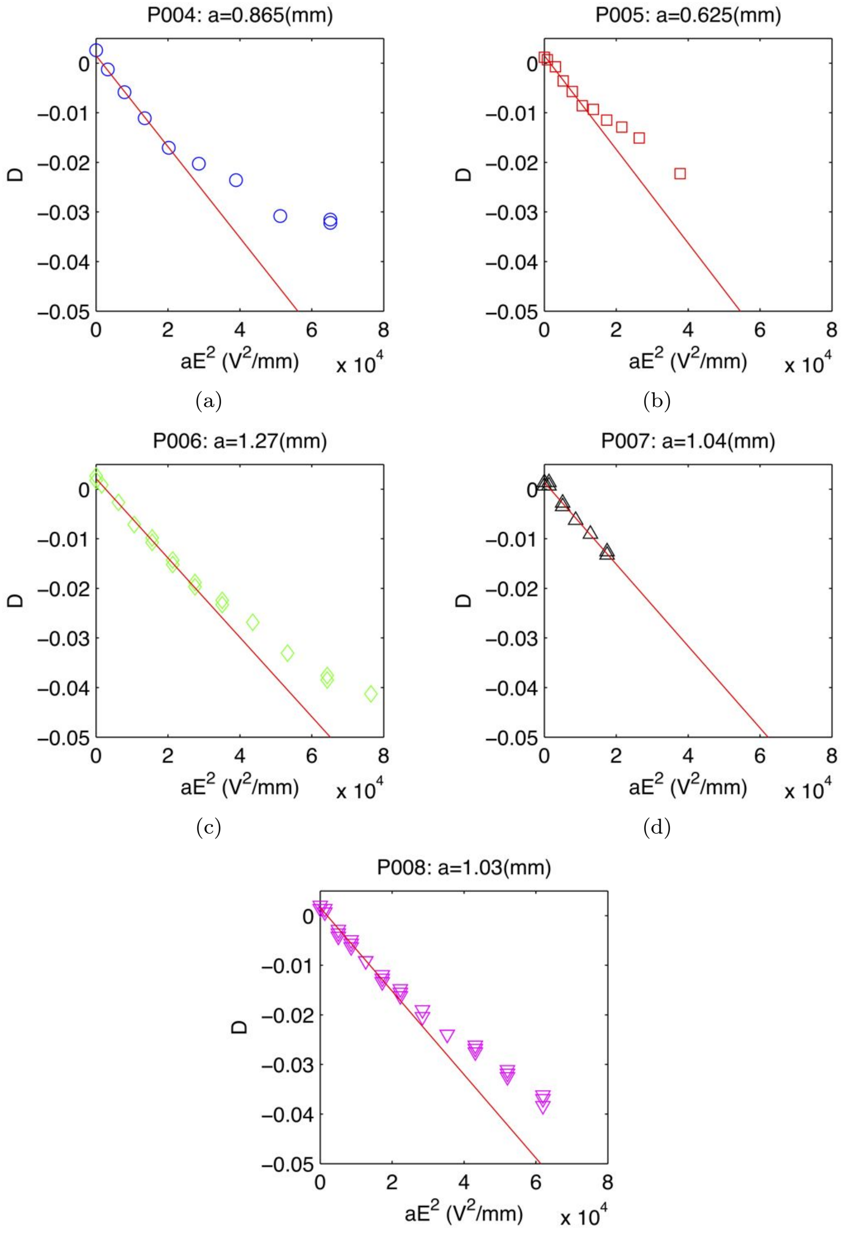

(a) (b) (c) (d) (e)

Figure 11: Linear regression of deformation D of 10 cSt silicone oil droplets in pure castor oil as function of aE^2. Points included in the line fit have applied electric field of 130V/mm and less, a total of 6 points per droplet including the point for no field (except only 5 points for P004, since the next reading is at $E = 153$ V/mm).

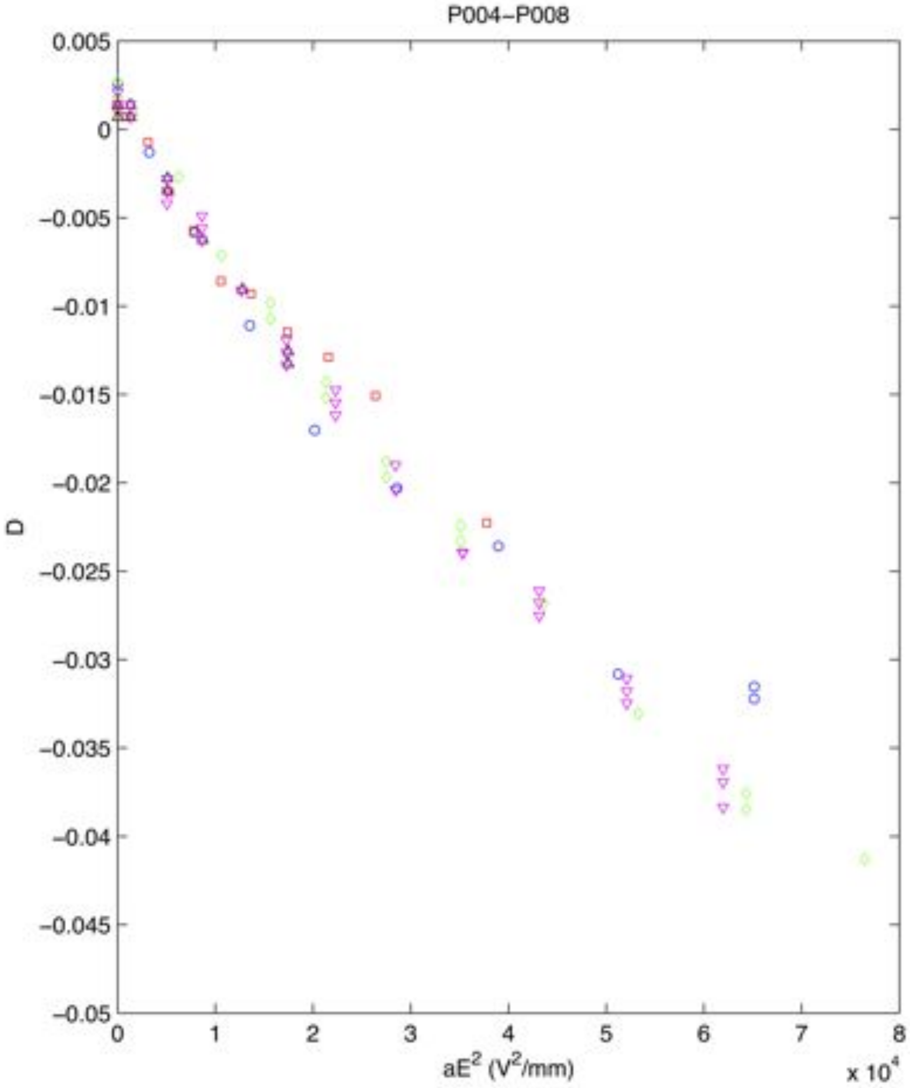

Figure 12: The data from Figure 11 gathered in one window. Repeatability is interpreted to be quite reasonable, especially for low fields.

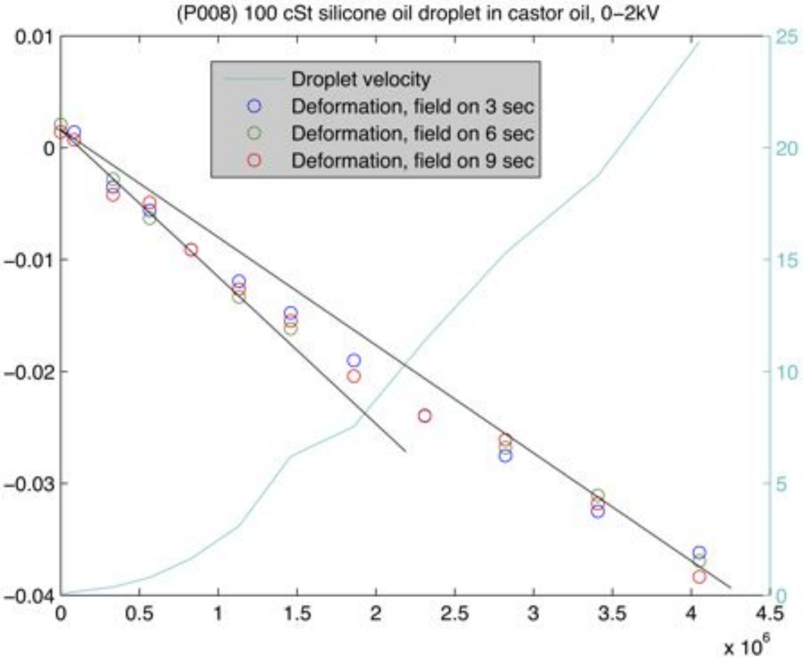

Figure 13: Deformation (left vertical axis) and velocity (pixels/seconds, right vertical axis) as a function of E^2. The straight lines are merely visual guides. The velocity scale of 0-25 px/s is equivalent to 0-0.072 mm/s, as seen in the scale of Figure 14. Deformation is plotted for 3, 6 and 9 seconds after the electric field is applied.

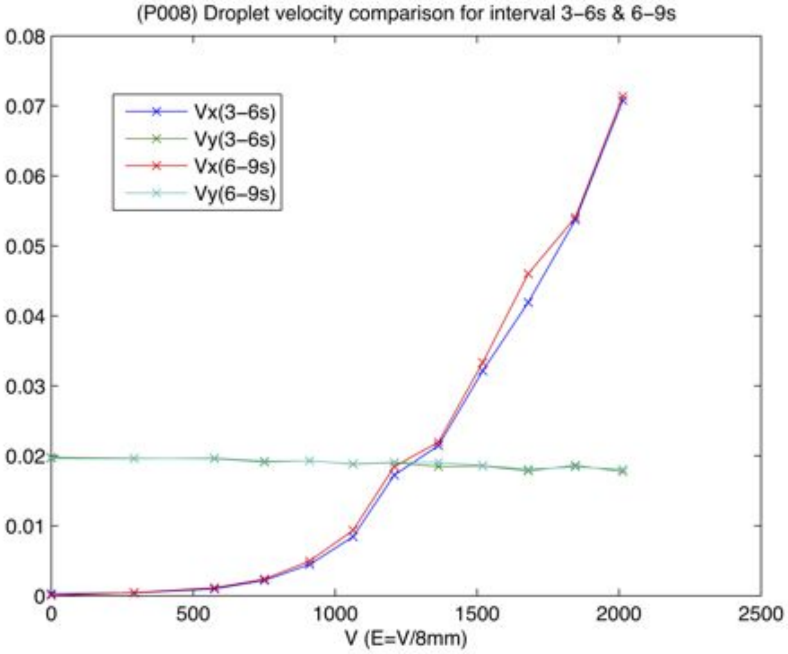

Figure 14: Velocity (mm/s) vs. electric field (V/8.2mm). Vertical and horizontal component of droplet drift velocity measured in the intervals 3-6 seconds after applied field and 6-9 seconds after applied field.

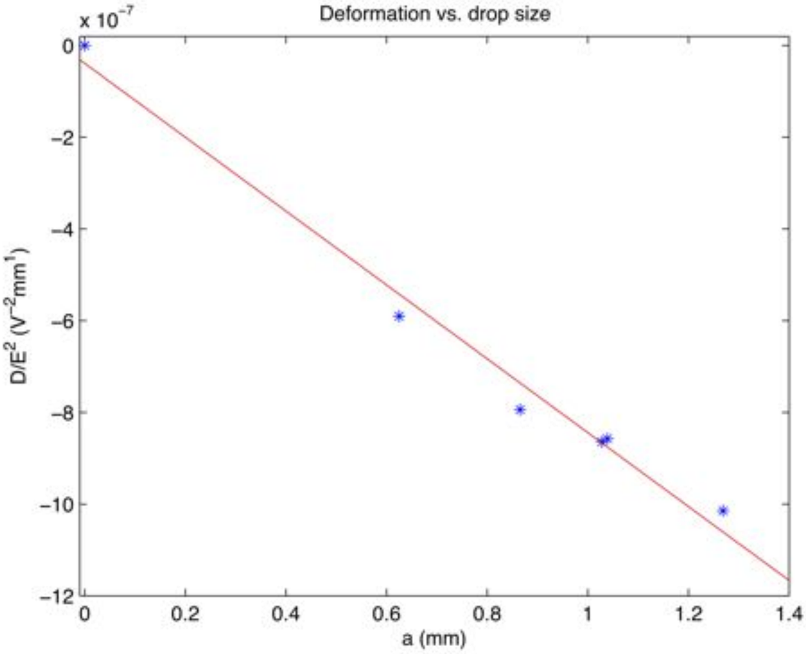

Figure 15: Deformation as a function of drop size, where each point is the deformation of a separate drop per E^2 (the line fit from Figure 11). The straight line is meant as a visual guide for evaluating the linearity of the points. The origin is marked as a data point, and the straight line is a linear fit of all the points.

5.1.2 Deformation when Laponite clay is added

Adding Laponite clay to the silicone droplet affects the droplet deformation surprisingly little in this regime where small deformations are studied. In Figure 16, 1.5% Laponite by weight is added to the droplet and the deformation is studied by the same method as for pure silicone droplets to which the clay sample is being compared. Unlike for the pure oil droplets, multiple deformation readings taken in an interval of a few seconds tend to become less oblate sequentially at the highest field values. This observation encourages a logging of deformation as a function of time.

In Figure 17 the applied field is 120 V/mm and deformation is graphed as a function of time, in seconds. The dynamic response does not distinguish itself from the response of pure oil droplets. However, in Figure 18, the field strength is doubled, and the reduction in oblate deformation over time is confirmed. The reason for the interruption of this deformation reduction at the 13 (s) mark is unknown, but it is noted that the droplet is moving closer to one of the electrodes. While this is not uncommon for a droplet, it is likely that the field is weaker near the electrodes, in the two regions closest to the electrodes, extending a quarter of the inter-electrode distance each[17]. It is worthwhile to use the information from Figure 18 to evaluate the deformation at the highest applied field point of Figure 16, since both figures are based on the same series of measurements.

Laponite clay is known to stretch droplets in a prolate manner. The dynamic measurement of deformation when 3% Laponite is added by weight is given Figure 19. Given a longer response time, this droplet deformation is prolate, in contrast to when 1.5%w/w Laponite or no clay is added. It is interesting to learn the significant difference in time scale for the deformation of clay particles. Laponite consists of 1nm platelets aggregated into somewhat larger particles, and they are much larger than molecules of the oil which dielectrically polarize in the applied electric field. The difference in time scale for polarizing the particles of clay to that of the oil molecules is perhaps trivial, however the viscous flow process which is the only process contributing to oblate deformation is slower than the dielectric polarization of the fluid, shown by a study of alternating fields[12].

Surprising, also, is the fact that the prolate deformation of Figure 19 is increasing so steadily over a long time period. Note that this time dependence, although obvious from the graph, is not noticeable by naked observation of the drop. The field was turned off prematurely for this reason, and the behavior is discovered long after experiments are performed. Extrapolating the linear region of increasing prolate deformation towards the starting point of applied electric field, one can see that the extrapolation does intersect the spherical deformation value at the point of time when the field is turned on! From this observation it is tempting to reason that the viscous flow process responsible for the initial oblate deformation is inhibited by chain formation. However, this level of electric field is at least half of what is expected for beginning chain formation. Within the narrow focus dept, chains are not visible either, despite plenty of illumination into the drop in this case. Nevertheless, inhibition of internal fluid flow would explain the behavior of the curve with respect to the extrapolation.

In the upper photo in Figure 20, the applied field is the same as in the dynamic sequence of Figure 19, however the drop has also been exposed to higher fields prior to this state. The field has been applied for an extended period, and the clay particles have structured themselves much like in a solid. This lumping of clay particles is possibly the gradual process indicated by linear increase in the prolate deformation. It also inhibitis some extent of viscous flow. The formation of lumped clay particles and stretching them into chains i easily repeated and reversed for this droplet. Nevertheless, let it be emphasized that these observations need to be repeated with properly varied parameters, since such a limited set of observations easily leads to over-generalized conclusions.

Another relevant fact, is that conductivity of the clay behaves in much the same way as the deformation; below a threshold field similar or lower than the critical field of chain formation, the conductivity is similar to a sample without any clay. However, over the threshold, the conductivity increases steadily, and not stopping within the measuring time of 10 minutes! When applying an electric field of 280 V/mm to 1.5%w/w Laponite in silicone oil, the current through the conductivity cell decreased from 0.5 to 0.45 nA in approximately one minute, but then increased steadily to 3.5 nA in 10 minutes. Comparing to Figure 22, this current corresponds to the same conductivity as for the surrounding castor oil. Consider the fact that the viscous flow driving an oblate deformation requires a higher conductivity outside the drop. Then it seems obvious that increase in conductivity inside the droplet is a highly likely mechanism for alteration of viscous flow.

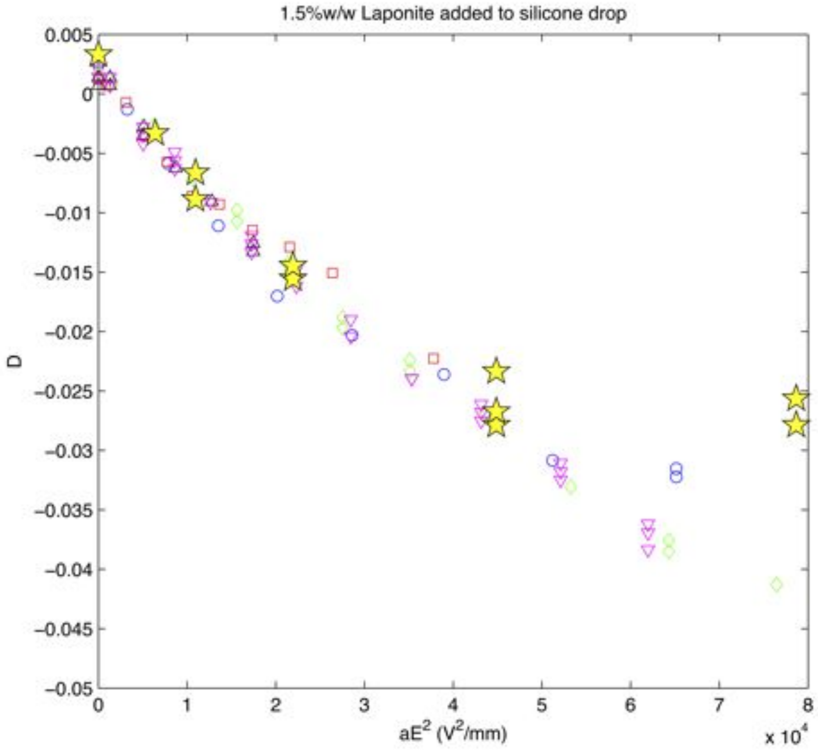

Figure 16: Yellow stars: Deformation as a function of aE^2 when 1.5% Laponite clay is added by weight to silicone drop submerged in castor oil. The size of the droplet is 1.31 mm, close to the pure silicone droplet whose marker is a green diamond shape. Interestingly, the deformation seems weakened at higher field values, but not at all in the lower field range. It is noted that the measurements taken when the field has been on for the longest, a couple of seconds longer, has the weakest deformation (except for the third strongest field, where only one increment separates the two deformation values). At the highest field strength, for instance, two pixel increments separate the deformation measurements. (Resolution could possibly be doubled by using a higher magnification on the microscope, however the droplet fell noticeably faster with clay, making free space inside the frame under the droplet more necessary).

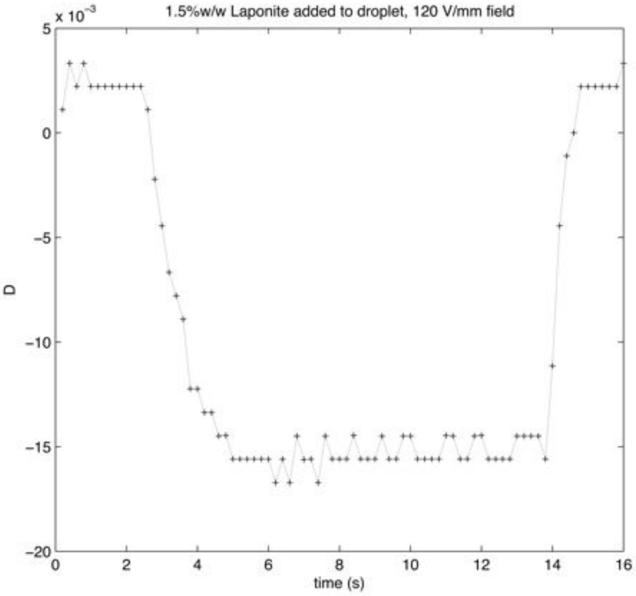

Figure 17: Deformation as a function of time (seconds) when 1.5% Laponite by weight is added to the drop, the same drop as in Figure 16. The applied field is 120 V/mm.

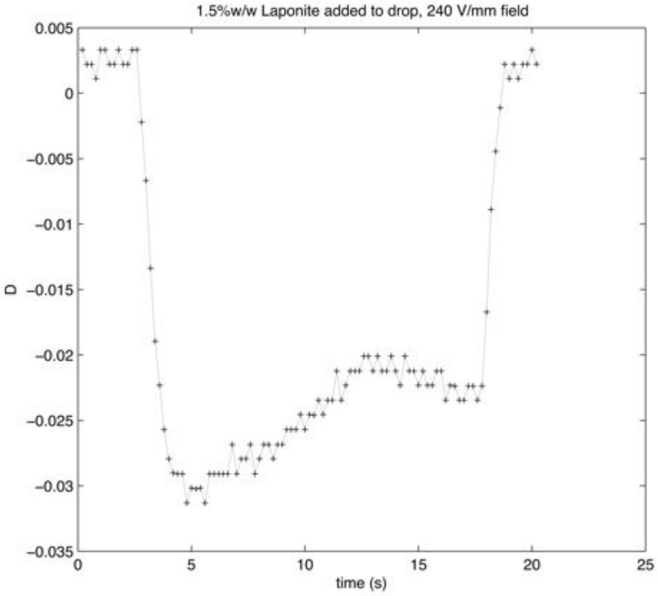

Figure 18: Same drop as in Figure 16 and 17, however applied field is doubled to 240 V/mm. The bend at 13 (s) might be due to the droplet moving closer to the electrode where the field is possibly reduced by ion concentration.

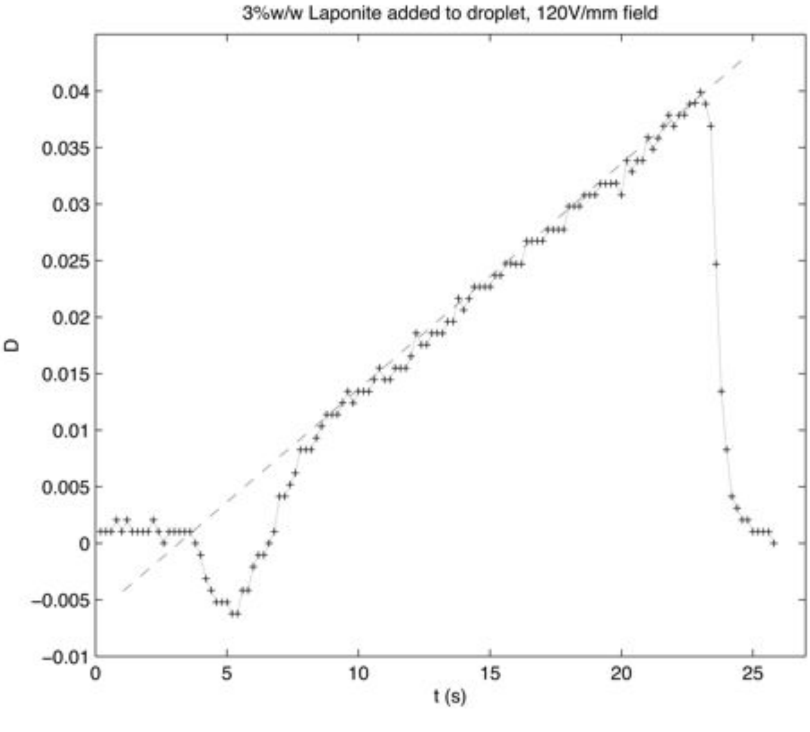

Figure 19: Deformation as a function of time (seconds) when 3% Laponite by weight is added to the 100 cSt silicone drop submerged in castor oil. The applied field is 120 V/mm.

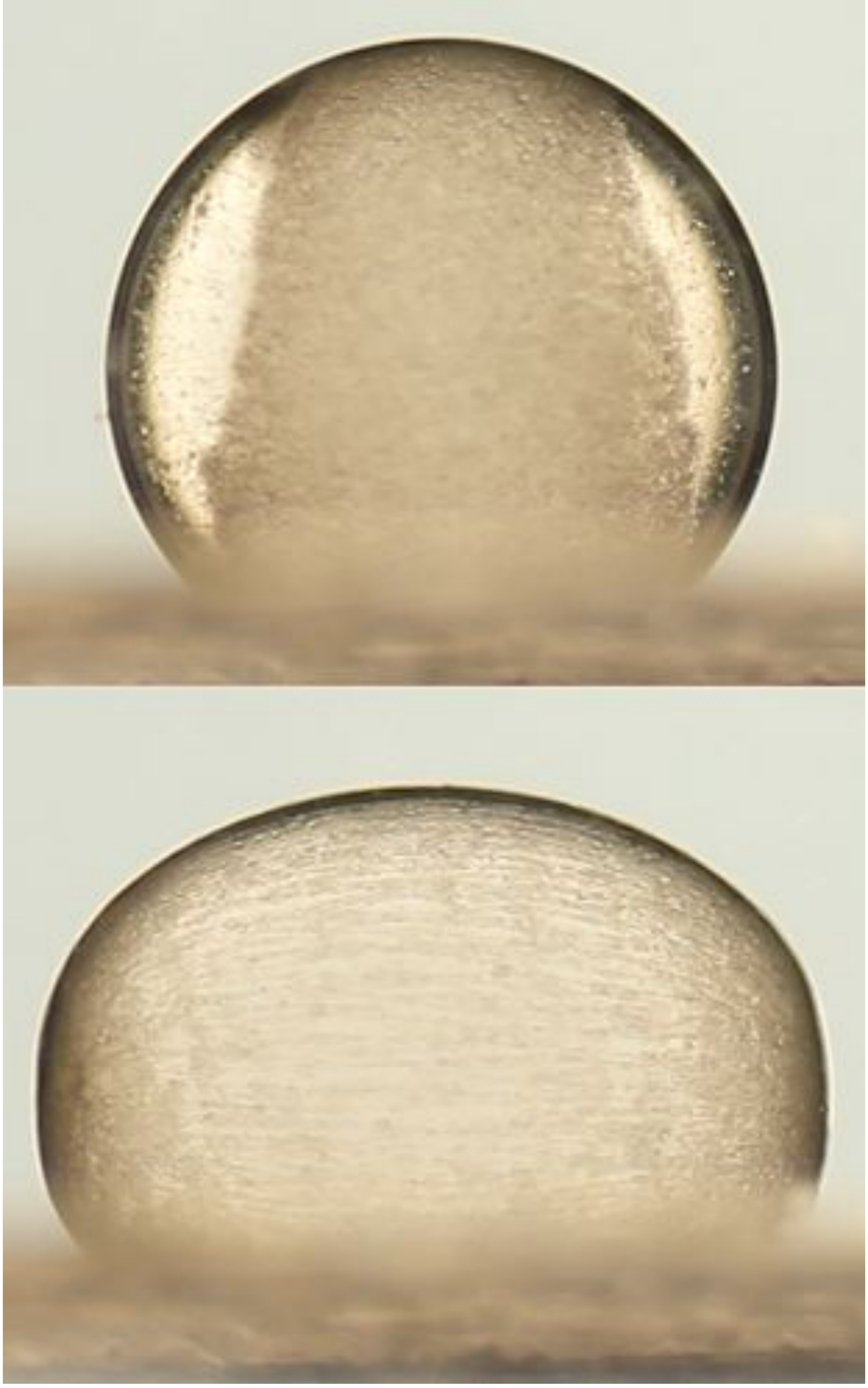

Figure 20: Photos of the droplet measured in Figure 19 after it has sunk to the bottom. In the upper photo, applied field is 120 V/mm, same as for the dynamic deformation sequence. In the lower photo, the field has been quadrupled, nearing 500 V/mm.

5.1.3 Electrodes outside sample cell

In order to apply the electric field and isolate its effect from phenomena of the electric currents, an experiment is performed with the electrodes outside the plastic cuvette, Figure 21. An initial attempt resulted in oblate deformation, indicating that current was still conducting through the plastic walls (!). Thus, a 1mm air gap is used between the copper electrode and plastic cuvette. Video from the microscope shows a 2-3 second long pulse of oblate deformation when the field is turned on, and almost equally strong oblate pulse when the field is turned off. However, both before the field is applied and after equilibrium is reached with the field on, deformation is non-existing. A potential difference of 9.5 kV is applied across the 13.5 mm electrode gap. The drop radius is $a = 2.5$mm. The resolution of the deformation measurement is 0.0007, and three measurements were conducted at least 1 second apart, both for field off and at drop equilibrium after applied field. All six readings were zero, meaning pixel identical height and width of the drop.

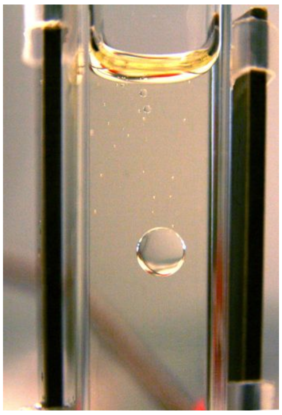

Figure 21: Sample cell with electrodes on the outside. Preliminary droplet attempt, not the actual microscope measured droplet.

The field between the electrodes is 700 V/mm when excluding effects of the dielectric oil, etc. Taking into account the reduced field due to dielectric properties of the oil possibly reduces the field to 460 V/mm inside the oil. A relative permittivity of 1 for the cuvette has been chosen for this calculation, since it yields the lowest field inside the oil. Choosing a higher relative permittivity for the cuvette results in a stronger field in the oil for such an oil region dominant geomtery. The deformation predicted by the perfect dielectric model, neglecting the possibility of currents, is $D = 0.08$ for the reduced field. In comparison, the oblate deformation is typically weaker than $D = -0.05$ for oblate deformations. In other words, the substantial prolate deformation predicted by the perfect dielectric model is non-existing in this experiment. A likely explanation is som sort of charge migration effect, possibly canceling most of the field. The dynamics of the oblate deformation pulse is comparable to the time dependence of the silicone oil conductivity, as discussed in Section 5.2.

5.2 Conductivity and permittivity

5.2.1 Drifting conductivity measurements

Some samples exhibit a time dependent current measurement after the potential difference is applied, and the effect is especially strong in silicone oil. The reduction in current reading over the first few minutes cannot be due to capacitive charge of the sample cell, since the time constant $\tau_0 = R_s C_{cell}$ is of the order $\approx 10^{-6}$ seconds, where R_S is the 6.8 MΩ series connected protective resistance and C_{cell} is the capacitance of the sample cell (pF magnitude). The initial current of some 100 μA should die off in less than a tenth of a millisecond.

Turning off the potential difference for a short while and turning the potential difference back on results in a current reading closer to the starting point, with the same reductive time dependence. Reversing the field causes a starting point for current measurement approximately twice as high as the original starting point, and still reducing with time in a similar manner as before.

The interpretation of this fall-off in current measurement is accumulation of charge carriers, i.e. charged molecules, at the electrodes which are unable to continue carrying current into the electrode. This charge material builds up at the electrode, reducing the field in the bulk of the fluid, further reducing the current through the sample. When evaluating the current readings, the initial reading is sought, and repeated application of the potential difference is performed with a few minutes of pause if more confidence in the current measurement is needed. However, results after repeating a measurement in this fashion indicates that there is a memory effect in the sample, and it is uncertain how long is needed for the sample to revert to the initial state before any potential difference was applied. Nonetheless, the initial reading is believed to be the most relevant, since charge buildup is part of the drop deformation process in the leaky dielectric model.

In some cases the drift in current readings increased as well, however this might be due to lack of both using detergent with excess rinsing as well as ultrasonic bath to remove detergent and other remains from the electrode prior to adding new sample.

5.2.2 Castor oil and mix of castor and corn oil

The plant oils provided a nice ohmic resistance, and the linearity in the conductivity of the castor oil and the even mix of castor and corn oil is shown in Figure 22. Each of these two fluids are are used as surrounding liquids in the drop systems studied. The conductivities calculated from the regression analysis of Figure 22 are included in the summary below, along with measured permittivity of the samples. The conductivity of the mixed oil sample was quite stable, however some drifting in the picoammeter reading was observed in the castor oil measurement.

5.2.3 Silicone oils

The conductivities of the silicone oils (10 and 100 cSt) were impossible to measure initially. Early conductivity measurements of both 10 and 100 cSt silicone oil samples were interpreted to be too small for the measurement method to

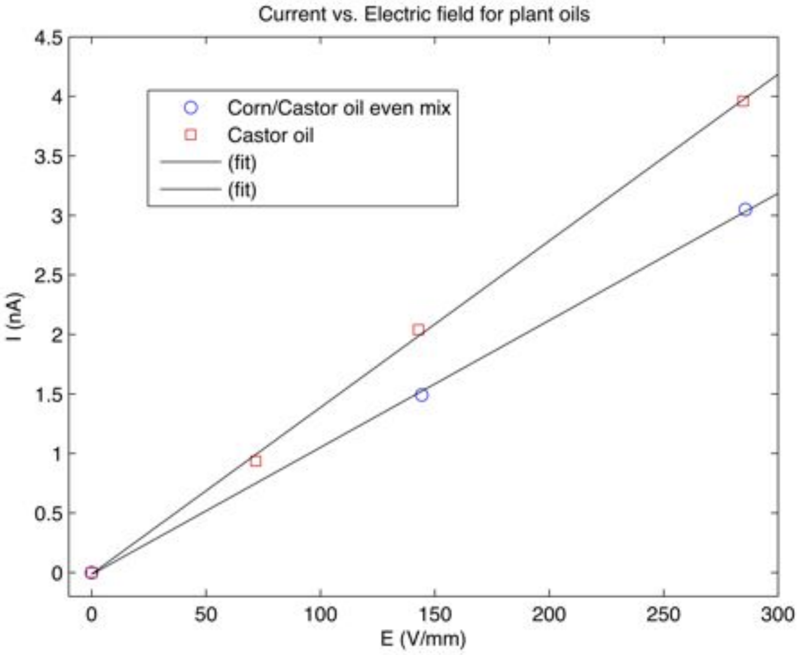

Figure 22: Measured current (nA) on the vertical axis as a function of applied field strength (V/mm) on the horizontal axis. The linear regression is not forced to go through the origin, however the origin is included as a measurement point. The castor oil is measured at 72, 143 and 285 V/mm, however with an extra uncertainty in the absolute value of a few percent due to the fact that glue remains were found on the electrodes post measurement. Unable to redo the measurement, an adjustment of 20% increase in conductivity has been made based on conductivity measurement of one similar sample performed both with and without the glue residue on the electrodes. The linear relation is nevertheless convincing. The even mix of castor and corn oil was only measured at 144 and 286 V/mm, however without glue residue on the electrodes.

detect. However, it was discovered with the 10 cSt silicone oil, that the conductivity rapidly falls off after the potential difference is applied. This makes the measurement difficult to assess. The rapid fall-off in the conductivity measurement was noticed in the 10 cSt silicone oil on the last day of the availability of the picoammeter, and it became impossible to redo the conductivity measurement of the 100 cSt silicone oil due to lack of time.

The first value returned from the picoammeter filter, meaning the median of the first 11 readings performed by the picoammeter, is approximately half a nano-ampere for 10 cSt silicone oil, and it is halved in as little as 10 seconds! If attention is not paid to the reading *while* the potential difference is turned on, the reading will be mistaken for noise that dies away. (Note: movement while managing the equipment raises the noise level, and a few seconds of keeping still is normally beneficial before recording measurements).

In lack of a setup that records all readings from the picoammeter as function of time automatically, the best procedure was to use the first value returned from the median filter of 11 readings. This merely estimates the order of magnitude of the conductivity of the silicone oil, however it also shows the non-ohmic nature of the conductivity, since the conductivity is calculated to be higher at the higher field strength. In other words, the current increases more than proportionally to the applied potential difference.

5.2.4 Summary

Sample	Relative permittivity ϵ_r	Conductivity σ (pS/m)	Field strength for conductivity measurement (V/mm)
50% Castor-, 50% Corn oil	2.82	33.5	(linear)
10cSt Silicone oil	2.1	~ 3	150
		~ 5	300
Castor oil	3.37	45*	(linear)
100cSt Silicone oil	2.13	unknown	-

*) Glue residue was on the electrodes. Correction adjustment has been performed based on measurement of another sample, the even mix of castor and corn oil, before and after the glue was removed.

Uncertainty is in the last digit.

6 Discussion

6.1 Conductivity and permittivity results

The resulting ratio of permittivity for castor oil over 100 cSt silicone oil is within 1-2% of the value quoted for Vizika et al.[12]. Quite interestingly, they have measured conductivity in the same manner as here, meaning that this study and Vizika et al. independently found the same design for measuring low conductivities. Note that they do not quote any specific value for conductivities of castor or silicone oil, despite claiming to pay careful attention the conductivity measurements. The ratio of conductivity R for silicone oil over castor oil is only specified to be less than 10^{-2}[12]. Here, the conductivity ratio for 10 cSt silicone oil is evaluated to be approximately $R \approx 10^2$, but depending largely on what time scale is considered relevant. Unfortunately, the conductivity of 100 cSt silicone oil was not measured on the small time scale of a few seconds after the potential difference is applied. Since the conductivity of silicone oil reduces rapidly the first few seconds after electricity is applied to the sample cell, using the digital interface and logging every measurement prior to digital filtering would greatly improve the data on which to evaluate the conductivity of silicone oil. In order to reduce noise in the measurement, a Faraday cage is suggested for future improvements.

6.2 Comparison with the leaky dielectric model

In order to compare the deformation of pure silicone droplets in castor oil to the leaky dielectric model, Eq. (2.21) can be divided in the following way:

$$\begin{aligned} m &= \frac{D}{aE^2} \\ m^* &= \frac{9}{16}\frac{\epsilon_{out}\epsilon_0}{\gamma}\frac{\Phi}{(2+R)^2} \end{aligned} \tag{6.1}$$

where Φ is defined in Eq. (2.21). Then the slope m of the linear regression of D vs. aE^2 should equal m^* according to the theory. The linear regression in aE^2 for droplets P004-P008 are summarized below.

	P004	P005	P006	P007	P008	Average
m (10^{-10}mV^{-2})	-9.18	-9.44	-7.99	-8.25	-8.40	-8.65
Droplet radius a	0.87	0.63	1.27	1.04	1.03	0.965

Note that a smaller droplet generates a steeper linear regression, without exception. This can also be deduced from Figure 15.

The chosen parameters for calculating m^* and the calculated value for m^* is given in the table below

ϵ_{out}	γ[12]	G	R	$\lambda^{(*)}$	m^*
3.37	$4.6 \cdot 10^{-3}$ (N/m)	0.625	10^{-2}	0.1	$-9.22 \cdot 10^{-10}$(mV^{-2})

(*) Estimated viscosity ratio, not measured

The average measured deformation is 6% lower than the prediction of the leaky dielectric model. The prediction is within the experimental variation of the 5 droplets compared; droplet P005 (the smallest one) deforms more than predicted for its size. The comparison is satisfying, however a good match between theory and measurement should not dazzle from the uncertainties of the experiment.

The parameters in calculating m^* in the table above are the parameters estimated before the outcome of the prediction was known. Although the ratio of permittivity G agrees with Vizika and Saville[12], they quote the permittiviy of castor oil, ϵ_{out}, as 4.45. Using their value in the calculation results in a value $m^* = 1.22 \cdot 10^{-9}$ (mV^{-2}), which makes the average measured deformation 30% lower than prediction.

Surface tension γ is understandably uncertain also, and an increase in surface tension of 10% reduces the estimate of deformation by 10% as well. Since measurement attempts of surface tension were unsuccessful, the value quoted by Vizika and Saville[12] is used.

The uncertainty of conductivity in silicone oil is already debated. If the relevant conductivity measurement of silicone is only a factor 10 less than castor oil, then $m^* = 7.4 \cdot 10^{-10}$ (mV^{-2}), whereas if it should in fact be 1000 times less, then $m^* = 9.4 \cdot 10^{-10}$ (mV^{-2}).

The deformation is only weakly dependent on the viscosity ratio λ, and the castor oil is estimated to be 10 times more viscous than the 100 cSt silicone oil.

6.3 Other experimental suggestions

The sample cell and electrode distance for studying droplet deformation could be substantially larger. As mentioned earlier, only the middle half of the region between the electrodes exhibited a homogenous field in the study by Hiromi et al.[17]. It is expected that increasing ion gradient in the quarter regions close the electrodes is the cause of the reduced field. The reduction in field due to ion gradients is an important source of systematic error in the measurement of deformation. Careful attention was also paid to the position of the drop in distance from the microsope, however it was sometimes very challenging to asses whether the droplet was in the middle of the electrode region, and not near the front or back wall of the sample cell.

Altering the humidity of clay is an efficient way of controlling conductivity and response to electric field. Drying the clay inhibits much of the response in terms of chain formation. On the other hand, clay which has been exposed to 97% humidity a couple of days forms chains much more easily. This is confirmed when measuring the conductivity. The conductivity with added humidity is higher right away (around 20 nA current in the cell), and increases fast and steadily for at least 15 minutes (reaching 250 nA current in the cell, see Figure 22 for comparison). The electric field applied is only 95 V/mm, a level which exhibits a lower, constant conductivity when the clay is not exosed to humidity.

The use of a fixed voltage selector was a crucial design decision. Without the fixed potential difference scale, systematic investigations would be practically impossible. However, learning the need to study dynamics and determining the exact frame off initiated potential difference, a much better idea emerged. The power supply should have been controlled by a digital acquisition card, so that the sequence of potential difference could be controlled from a computer script.

At higher fields, however, when drop migration dictates the need for switching direction, etc., possibility for manual interruption is needed.

The pendent drop experiment for determining interfacial tension is worthy of a second attempt. The sunflower oil in which the 100 cSt silicone oil was submerged pending from the burette is less dense than the 10 cSt silicone oil, but the exact density has not been measured. The density of castor oil which has been ordered since, is at least 5 times closer to the density of 100 cSt silicone oil. Pending the 100 cSt silicone oil droplet into castor oil will give an at least 5 times bigger pendant drop, depending on exactly how light the sunflower oil used earlier was. Note that the high viscosity of the castor oil will demand patience, and the tip of the burette should be smooth in order to have a stable connection to the droplet.

6.4 Suggestion for future study

A systematic study of different clay samples, varying humidity, concentration and clay type would be a suitable extension of the experiments conducted here. The deformation response time as well as deformation as a function of electric field has proven to provide new insight, and should be extended to other clay samples.

A Appendix

A.1 Solution of Laplace equation for dielectric sphere

In spherical coordinates with a symmetry axis, the Laplace equation of Eq. (2.3) can be written

$$\frac{\partial}{\partial r}\left(r^2\frac{\partial V}{\partial r}\right)+\frac{1}{\sin\theta}\frac{\partial}{\partial\theta}\left(\sin\theta\frac{\partial V}{\partial\theta}\right)=0 \tag{A.1}$$

Separating variables, we set $V(r,\theta)=R(r)\Theta(\theta)$. Putting this into Eq. (A.1) and dividing by V, the equation becomes:

$$\frac{1}{R}\frac{d}{dr}\left(r^2\frac{dR}{dr}\right)+\frac{1}{\Theta\sin\theta}\frac{d}{d\theta}\left(\sin\theta\frac{d\Theta}{d\theta}\right)=0 \tag{A.2}$$

Since each term is independent of the other, ie. the first term depends on r while the second on θ, each term must be constant to satisfy the equation. We can then separate into two equations, the first of which is:

$$\frac{1}{R}\frac{d}{dr}\left(r^2\frac{dR}{dr}\right)=l(l+1) \tag{A.3}$$

with solution

$$R(r)=Ar^l+\frac{B}{r^{l+1}} \tag{A.4}$$

where A and B are arbitrary constants.

The second equation becomes:

$$\frac{1}{\Theta\sin\theta}\frac{d}{d\theta}\left(\sin\theta\frac{d\Theta}{d\theta}\right)=-l(l+1) \tag{A.5}$$

with one solution being the l'th Legendre polynomial in $\cos\theta$:

$$\Theta(\theta)=CP_l(\cos\theta) \tag{A.6}$$

where C is an arbitrary constant. The other solution to Eq. (A.5) for each l turn out to blow up at $\theta=0$ and/or $\theta=\pi$ and these components of the solution must always be set to zero when the z-axis is accessible[3].

Absorbing constant C into A and B, the most general separable solution to Laplace's equation is

$$V(r,\theta)=\left(Ar^l+\frac{B}{r^{l+1}}\right)P_l(\cos\theta). \tag{A.7}$$

This yields an infinite set of solutions, one for each l. The general solution to the Laplace equation is a linear combination of the separable solutions:

$$V(r,\theta)=\sum_{l=0}^{\infty}\left(Ar^l+\frac{B}{r^{l+1}}\right)P_l(\cos\theta). \tag{A.8}$$

The sum over separable solutions that do not diverge, hence the general solution, inside the sphere is

$$V_{in}(r,\theta) = \sum_{l=0}^{\infty} A r^l P_l(\cos\theta). \tag{A.9}$$

Outside the sphere with boundary condition (2.6) we have the uniform field along with separable solutions that converge to zero at infinity:

$$V_{out}(r,\theta) = -E_0 r\cos\theta + \sum_{l=0}^{\infty} \frac{B}{r^{l+1}} P_l(\cos\theta). \tag{A.10}$$

The boundary condition for continuous potential, Eq. (2.4), requires that

$$A_l a^l = \frac{B_l}{a^{l+1}}, \qquad \text{for } l \neq 1, \tag{A.11}$$

$$A_1 a = -E_0 a + \frac{B_1}{a^2}. \tag{A.12}$$

However, the boundary condition for the electric field perpendicular to the sphere surface, Eq. (2.5), requires that

$$\epsilon_{in} l A_l a^{l-1} = -\epsilon_{out}\frac{(l+1)B_l}{a^{l+2}}, \qquad \text{for } l \neq 1, \tag{A.13}$$

$$\epsilon_{in} A_1 = -\epsilon_{out}\left(E_0 + \frac{2B_1}{a^3}\right). \tag{A.14}$$

Thus

$$A_l = B_l = 0, \qquad \text{for } l \neq 1, \tag{A.15}$$

$$A_1 = -\frac{3}{\epsilon_{in}/\epsilon_{out} + 2} E_0 \tag{A.16}$$

$$B_1 = \frac{\epsilon_{in} - \epsilon_{out}}{\epsilon_{in} + 2\epsilon_{out}} a^3 E_0 \tag{A.17}$$

And the potential inside the sphere is given in Eq. (2.7). The field is illustrated in Fig. 1

A.2 Droplet velocity

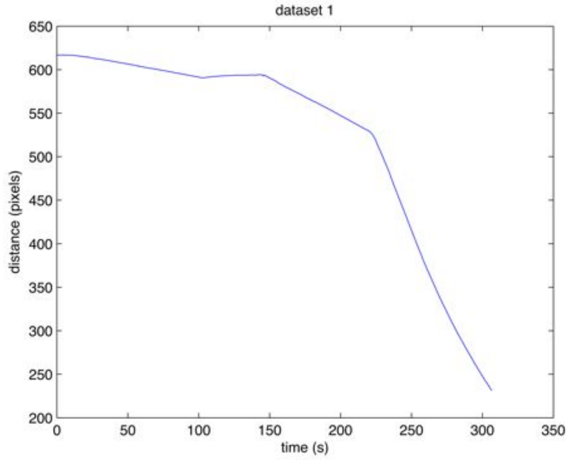

Figure 23: Tracking the position of the droplet. The droplet is very small. First, a low field is applied, then turned off. The droplet drifts in the opposite direction (!) while field is off. Next, two higher fields are applied sequentially.

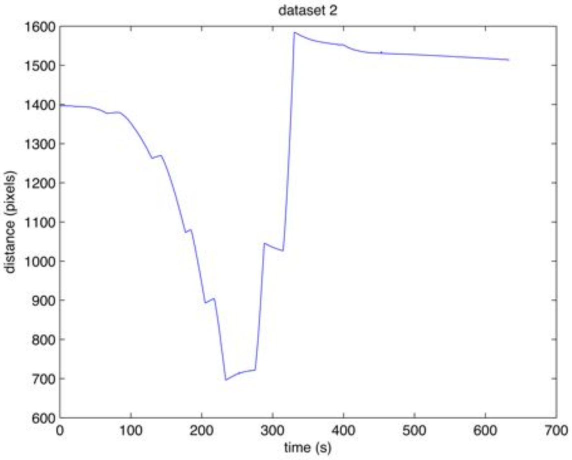

Figure 24: Similar behaviour for a bigger droplett. Field reversed midway.

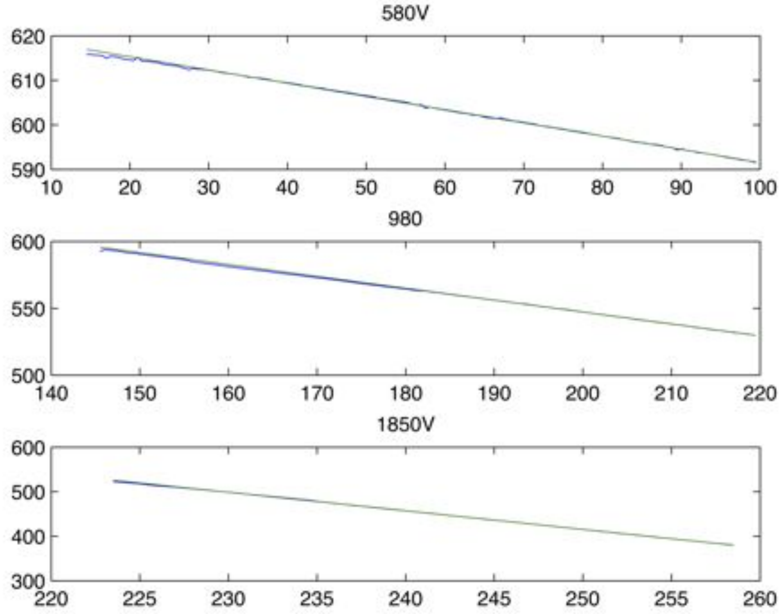

Figure 25: Determining velocity vs. field from Figure 23.

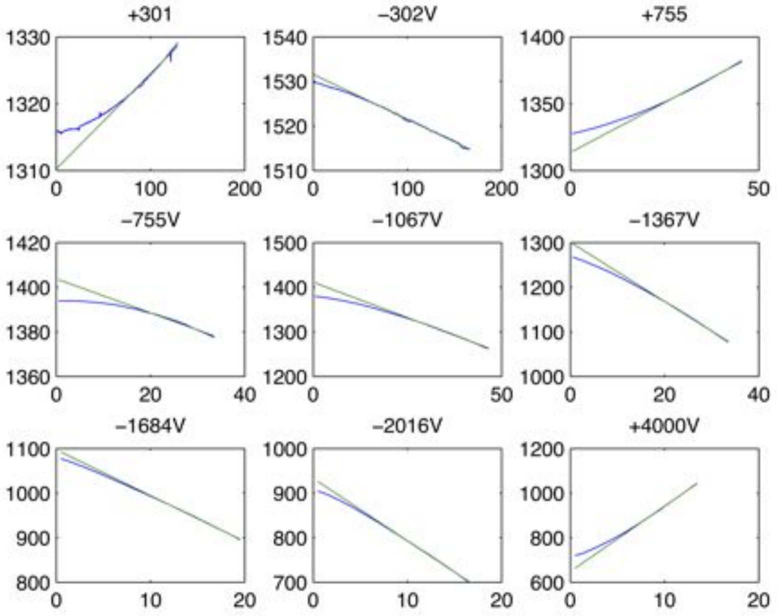

Figure 26: Determining velocity vs. field from Figure 24.

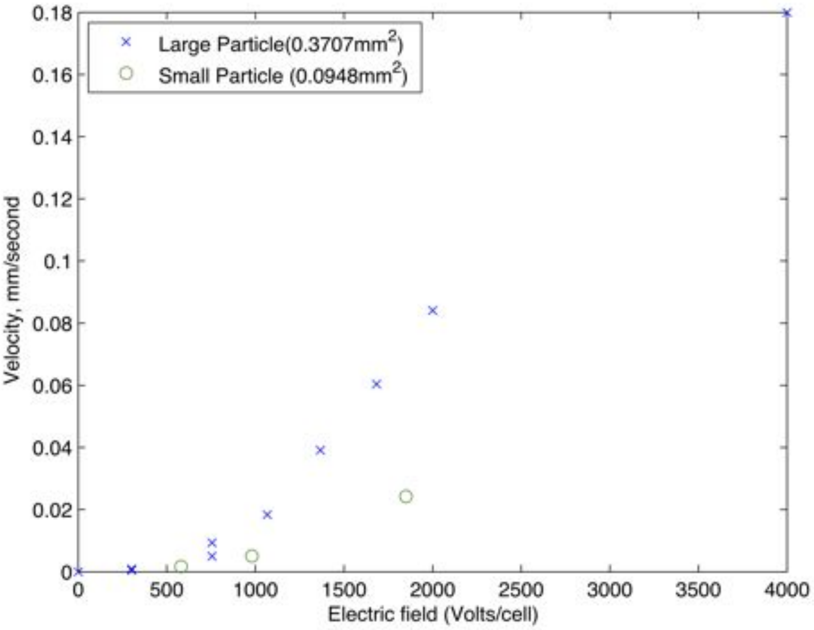

Figure 27: Velocity vs. field from Figure 23 (small droplet) and 24 (large droplet).

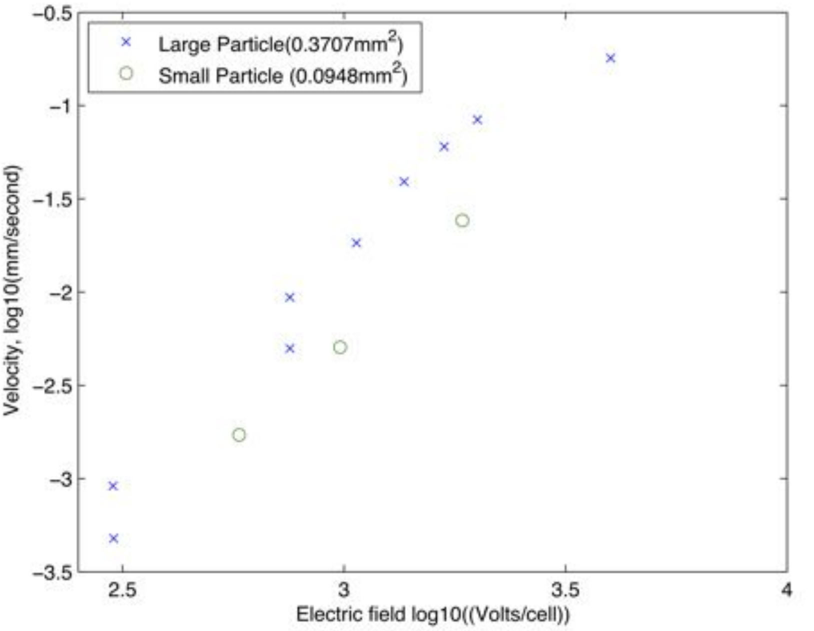

Figure 28: Log-log version of Figure 27.

A.3 Fluid flow velocity tangential to droplet

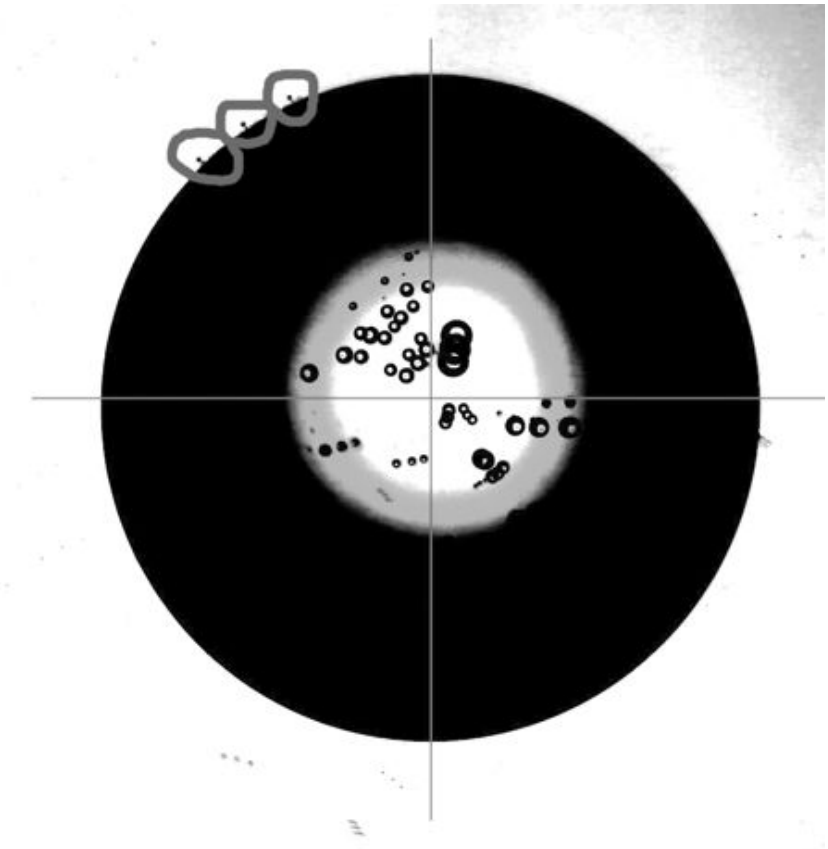

Figure 29: Droplet P008 with 92 V/mm applied field. The droplet has been repositioned and superimposed at t=3, 6 and 9 seconds after applied field. A small particle on the surface of the droplet is tracked in the upper left corner. (The dot inside the circles is actually drawn, but what resembles a line connecting the dot to the droplet surface is actually the physical particle). The distance covered in 6 seconds is 119 pixels = 0.341 mm, resulting in an average velocity of 0.057 mm/s. The angle between the line perpendicular to electrodes (horizontal line) and the position vector of the particle from the droplet center is 45.6°, 55.5° and 64.7°, respectively.

A.4 Plots of deformation from early experiments

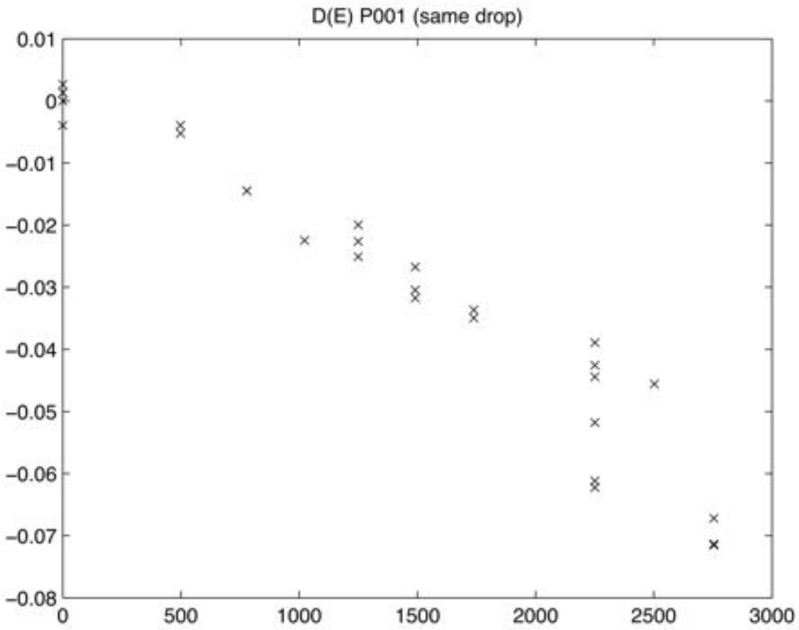

Figure 30: Deformation D as function of electric field E (V/8.2mm) (not squared). Droplet P001 consists of 10cSt silicone oil surrounded by gradient of castor and corn oil. The gradient is made from 50/50 mix of castor and corn oil as heavy phase, and the light phase mix is twice as much corn oil compared to castor oil. At 2250 V/8.2mm, the droplet moved both horizontally and vertically. Horizontal movement influenced the deformation towards prolate shape (less negative deformation) while vertical movement enhanced the oblate deformation.

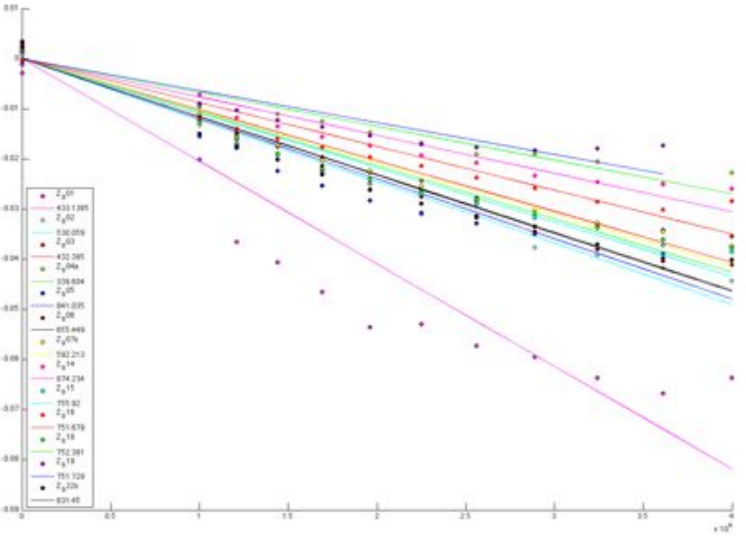

Figure 31: Initial measurements where the applied potential started at 1000V over 8.2mm and increased until 2000V. Movement of the drop due to field was later learned to be a problem, and the interesting lower range was omitted. Pictures were taken instead of video, and the allowed response time for deformation is unknown and possibly too short.

References

[1] C.T. O'Konski, H.C Tacher Jr. The Distortion of Aerosol Droplets by an Electric Field. *Journal of Physical Chemistry 57 9:955-958.* 1954.

[2] A.R. Thiam, N. Bremond, J. Bibette. "Breaking of an Emulsion under an ac Electric Field *Phys. Review Lett. 102:188304.* 2009.

[3] David J. Griffiths. Introduction to Electrodynamics, 3rd edition. *Prentice-Hall International, Inc.* 1999.

[4] D.A. Saville. "ELECTROHYDRODYNAMICS: The Taylor-Melcher Leaky Dielectric model" *Annu. Rev. Fluid Mech. 29:27-64.* 1997.

[5] G. Taylor. Studies in Electrohydrodynamics. I. The Circulation Produced in a Drop by Electrical Field. *Proc. R. Soc. Lond. A 291:159-166.* 1966.

[6] E.K. Zholkovskij, J.H. Masliyah, J. Czarnecki. An electrokinetic model of drop deformation in an electric field. *J. Fluid Mech 472:1-27.* 2002.

[7] J.Q. Feng. Electrohydrodynamic behaviour of a drop subjected to a stteady uniform electric field at finite elecgric Reynolds number *Proc. R. Soc. Lond. A 455:2245-2269.* 1999.

[8] J.O. Fossum. Physical Phenomena in Clays. *Physica A 270, 270.* 1999.

[9] J.O. Fossum, Y. Mêheust, K.P.S. Parmar, K.D. Knudsen, K.J. Måløy, D.M. Fonseca. "Intercalation-enhanced electric polarization and chain formation of nano-layered particles. *Europhys. Lett.*. 2006.

[10] Xize Niu, Mengying Zhang, Jiinbo Wu, Weija Wen and Ping Sheng. "Generation and manipulation of 'smart' droplets" *Soft Matter, 5:576-581.* 2009.

[11] B. Wang, M. Zhou, Z. Rozynek, J.O. Fossum. "Electrorheological properties of organically modified nanolayered laponite: (...)" *J. Mater. Chem. 19:1816-1828.* 2009.

[12] O. Vizika, D. A. Saville. "The electrohydrodynamic deformation of drops suspended in liquids in steady and oscillatory electric fields" *J. Fluid Mech. 239:1-21.* 1992.

[13] J.C. Baygents, N:J:Rivette, H.A. Stone. "Electrohydrodynamic deformation and interaction of drop pairs" *J. Fluid Mech. 368:359-375.* 1998.

[14] P. Lecomte, Du Noüy. "A new apparatus for measuring surface tension" *J. of General Physiology.* . 1919.

[15] H.H. Zuidema, G.W. Waters. *Ind. Eng. Chem. (Analytical Ed.), 13, 312.* 1941.

[16] C. Huh, S.G. Mason. *Colloid & Polymer Science, 253:266-580* . 1975.

[17] Hiromi Sato, Nobufuji Kji. "Behavior of blateley deformed droplets in an immsicible dielectric liquid under a steady and uniform electric field" *PHYSICS OF FLUIDS 18, 127101.* . 2006.